LOAD DISTRIBUTIONS IN BOLTED SINGLE LAP JOINTS UNDER NON-CENTRAL TENSILE SHEAR LOADING

by

CHAIWAT SINTHUSIRI

A doctoral research project submitted in partial fulfillment of the requirements for the degree of

DOCTOR OF PHILOSOPHY IN MECHANICAL ENGINEERING

2021

Oakland University
Rochester, Michigan

Doctoral Advisory Committee:

Sayed A. Nassar, Ph.D., Chair
Meir Shillor, Ph.D.
Xianjie Yang, Ph.D.
Zhijun Wu, Ph.D.

To our parents, my beloved wife, and daughters.

ACKNOWLEDMENT

Firstly, I would like to express my special gratitude and appreciation to my adviser, Professor Sayed A. Nassar for the continuous support of my Ph.D. study and related research, for his patience, encouragement, motivation, and immense knowledge. Your guidance on both research as well as my career have been invaluable.

Also, I would like to thank the members of my advisory committee Dr. Zhijun Wu, Dr. Meir Shillor and Dr. Xianjie Yang for their valuable time, helpful directions, and continuous support.

The author would like to gratefully acknowledge Dr. Sherif Gindy at Sensor Data for their support and providing the instrumented strain gage bolts. Also, William Heather my co-worker who fabricated the test fixtures for testing.

I also would like to thank Marco Gerini Romagnoli, my classmate, who assisted me for setting up the experiment and taught me to use the equipment at Fastening and Joining Research Institute (FAJRI) laboratory.

Finally, I would like to thank my family. I am deeply and forever indebted to our parents, my beloved wife, Aof and my daughters, Sammie and Silvie for their endless love, support, and encouragement throughout my entire life.

Chaiwat Sinthusiri

ABSTRACT

LOAD DISTRIBUTIONS IN BOLTED SINGLE LAP JOINTS UNDER NON-CENTRAL TENSILE SHEAR LOADING

by

Chaiwat Sinthusiri

Advisor: Sayed A. Nassar, Ph.D.

This study uses a numerically calibrated beam theory-based model to investigate the bolt load distributions in a preloaded two-bolt single lap joint under non-central tensile shear loading. The linear spring-based modeling is used for the two preloaded bolts and substrates. The bolt stiffnesses were derived from the bolt flexibilities influence by the bending deformation, the shear deformation, the bolt, and plate contact deformations. Due to the non-uniform load distribution along the bolt shank, the 3D finite element analysis was used to determine the correlation factors of each influence factors.

Non central loading may be due to geometric tolerances that would cause additional moment loading on the joint. Thus, the load would not be equally distributed among all bolts in the joint. The effect of various joint parameters, bolt preload and off-center location of the tensile shear loading is investigated and discussed.

TABLE OF CONTENTS

LIST OF TABLES

LIST OF FIGURES

NOMENCLATURE

$\boldsymbol{A_b}$	Cross section area of the bolt
$\boldsymbol{A_{pl}}$	Cross section area of the plate.
$\boldsymbol{C}$	Summation flexibility of the bolt
$\boldsymbol{C_{bb}}$	Bending flexibility of the bolt
$\boldsymbol{C_{bs}}$	Shearing flexibility of the bolt
$\boldsymbol{C_{bbr}}$	Bearing flexibility of the bolt
$\boldsymbol{C_{pbr}}$	Bearing flexibility of the plate
D	Bolt diameter
E	Edge distance of the plate
$\boldsymbol{E_b}$	Young's Modulus of the bolt
$\boldsymbol{E_x}$	Young's Modulus of the plate
$\boldsymbol{E_{x1}}$	Young's Modulus of the plate 1
$\boldsymbol{E_{x2}}$	Young's Modulus of the plate 2
F	Tensile Shear Loading
$\boldsymbol{F_N}$	Bolt Preload
$\boldsymbol{F_{bs}}$	Transverse shear force
$\boldsymbol{G_b}$	Shear modulus of the bolt

$\boldsymbol{I_b}$	Moment of inertia of the bolt shank cross section area
$\boldsymbol{I_p}$	Moment of inertia of the plate cross section area
$\boldsymbol{K_1}$	Stiffness of plate2 section from bolt2 to the end of plate 2
$\boldsymbol{K_2}$	Stiffness of plate 2 section from bolt1 to bolt2
$\boldsymbol{K_3}$	Stiffness of bolt 2
$\boldsymbol{K_4}$	Stiffness of plate 1 section from bolt1 to bolt2
$\boldsymbol{K_5}$	Stiffness of bolt 1
$\boldsymbol{K_6}$	Stiffness of plate 1 section from bolt1 to the end of plate 1
$\boldsymbol{K_p}$	Stiffness of plate
$\boldsymbol{L}$	Effective bolt length
$\boldsymbol{L_1}$	Edge distance of plate 1
$\boldsymbol{L_2}$	Edge distance of plate 2
M	Bending moment due to contact loading
$\boldsymbol{M_e}$	Bending moment due to eccentrically tensile loading
$\boldsymbol{P_1}$	Load distribution on bolt 1
$\boldsymbol{P_2}$	Load distribution on bolt 2

W	Plate width
e	Tensile loading offset distance from bolt center line
$\boldsymbol{p}$	Distance between bolt 1 and bolt 2
$\boldsymbol{r_e}$	Outer contact radius under bolt head
$\boldsymbol{r_i}$	Internal contact radius under bolt head
$\boldsymbol{t_1}$	Thickness of Plate 1
$\boldsymbol{t_2}$	Thickness of Plate 2
$\boldsymbol{u_1}$	Displacement of mass node 1
$\boldsymbol{u_2}$	Displacement of mass node 2
$\boldsymbol{u_3}$	Displacement of mass node 3
$\boldsymbol{u_4}$	Displacement of mass node 4
$\boldsymbol{u_5}$	Displacement of mass node 5
$\boldsymbol{u_6}$	Displacement of mass node 6
$\boldsymbol{w_1}$	Uniform load distribution between bolt shank and plate 1
$\boldsymbol{w_2}$	Uniform load distribution between bolt shank and plate 1
$\boldsymbol{\alpha, \beta, \gamma, \varphi}$	Correlation Factors
$\boldsymbol{\delta}$	Transvers displacement

$\boldsymbol{\lambda}$	Constant dependent of bolt underhead bending stiffness
$\boldsymbol{\mu}$	Static friction coefficient,
$\boldsymbol{\sigma_a}$	Normal Stress due to axial force
$\boldsymbol{\sigma_b}$	Normal stress due to bending moment
$\boldsymbol{\sigma_{avg}}$	Average normal stress

CHAPTER ONE

INTRODUCTION AND LITERATURE SURVEY

1.1 Introduction

The bolted lap joints are widely used in mechanical systems because it is relatively reliable to transfer higher loads and ease to assemble and disassemble for a maintenance. It also has ability to join dissimilar materials, relative low cost, the capability of creating a clamping force and higher fatigue resistance compared to other traditional joining methods such as threaded fasteners, welding, rivets and adhesive bonding.

In many mechanical applications where the bolted lap joints have multiple bolts fastened to the substrates and some cases, those substrates have different thicknesses or dissimilar materials. The lap bolted joints are also subject to the possible external loads: shearing, bending, tensile, or vibration fatigue. The substrates or the bolts may damage or have the clamp load lost. This depends on the bolted lap joint strength capacity and the bolts load sharing.

To ensure the reliability, the safety and the durability of the bolted lap joint, the bolt load distribution determination has been widely studied because it plays a significant role in any joint failure analysis. The bolts load sharing may not be equally shared due to different bolt diameter, the substrates geometries, and the external load application location.

1.2 Literature Survey

Khashaba et al. [1] studied the effect of washer size and tightening torque on bolted joint in composite structures. Experimental results from the shear test machine shown that decreasing the contact pressure by increasing the washer size could result the lower bearing strength. Although the bearing strength of the joint increases with the increasing the tightening torque.

Pakdil [2] performed the experimental failure analysis of the bolted joints in laminated plates under tensile loads found that the bearing strength of the joint increased with an increase in edge distance to diameter ration and/or in width to diameter. Increasing the applied bolt pretensions increase bearing strengths. The failure modes usually occur in four basic modes: cleavage, net-tensile, shear-out and bearing modes.

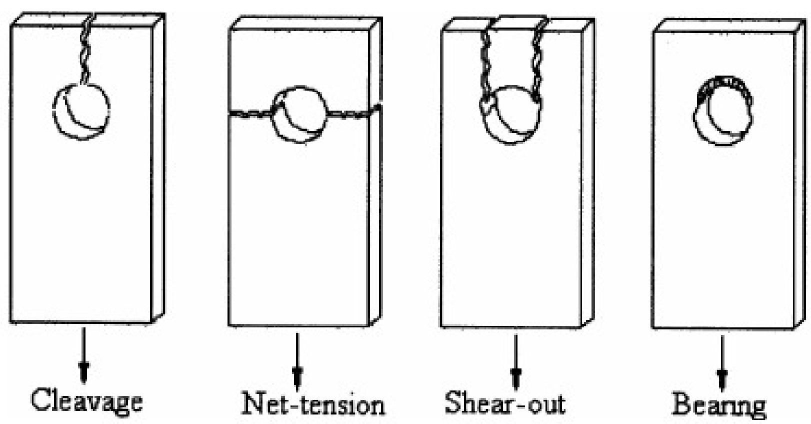

Figure 1.1 Failure mode in bolted composite plates [2].

Kweon et al. [3] studied the combined mechanical fastening and adhesive bonding of a double shear joints of carbon fiber and aluminum. Hybrid joining is effective when the mechanical fastening is stronger than the bonding.

McCarthy et al. [4] experimentally investigated the bolt-hole clearance effect on a single-bolt, single-lap, composite bolted joints. They found that increasing the bolt hole clearance reduces joint stiffness and bearing strength.

McCarthy et al. [5] also found that a tighter hole clearance in a single lap, multi bolted composite joint exhibits better on holding the load, but only 5% improvement. He also found the tighter fit joints have a longer fatigue life. The experimental studies in [3], [4] and [5] did not consider the tightening torque effect.

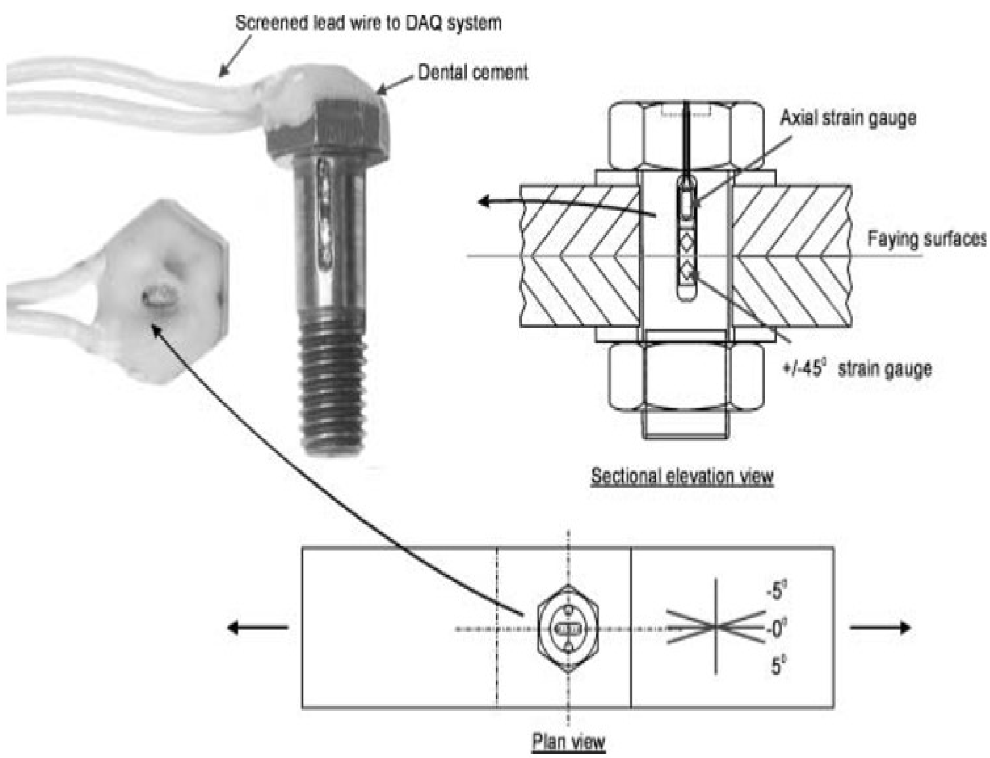

Figure 1.2 Instrumented bolt used for load distribution measurement [5].

Stocchi et al. [6] simulated the FE model of a single lap shear composite bolted joint with countersunk fasteners under static tensile load. According to the numerical and experimental data, the joint behavior can be divided in five stages as shown in Fig.1.2.

Liu et al. [7] developed a mass-spring based analytical model to predict the bolt load distribution in single lap thick laminate joints with zero bolt preload and under central tensile shear loading. He reported that the load distribution becomes more uneven when the thickness ratio increases.

Liu et al. [8] developed a modified instrumented bolt (MIB) to measure bolt shear loads in multi-bolt joints but the method was limited to specific bolt joint combinations.

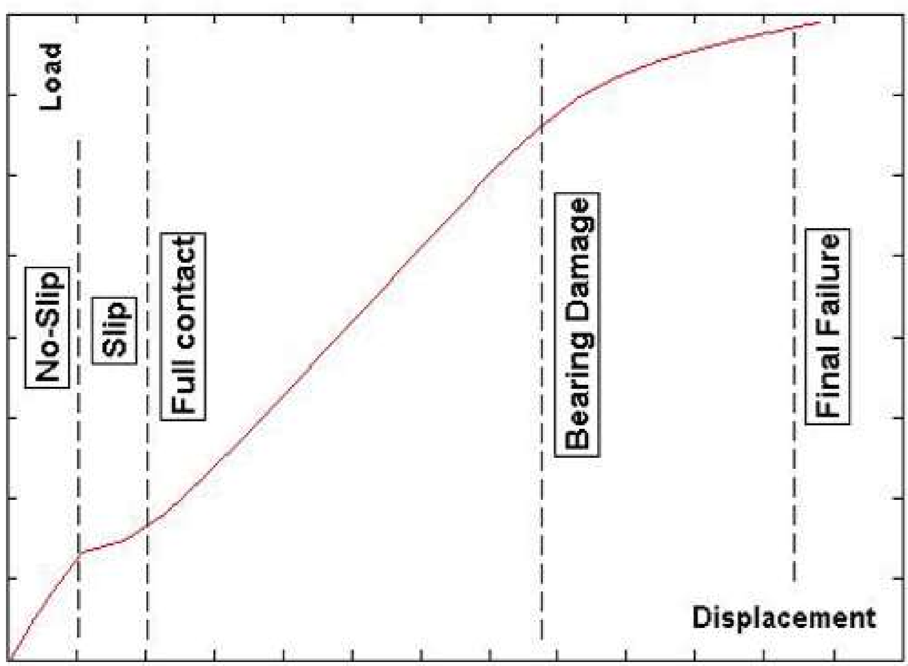

Figure 1.3 Illustration of single lap joint behavior under tensile loading [6].

Yeh et al. [9] studied several different fastener flexibility evaluation methods and found that a Lee modified NACA 1051 equation has a good improvement in load distribution prediction within 5%-10% error.

Lui et al. [10] developed 2D FEM to predict the loading sharing between the multi bolted joints. The beam elements are used to determine the shearing and bending flexibility of fasteners, whereas the bush elements are used to determine bearing flexibility between the fasteners and plates. The proposed 2D numerical method is more efficient compared with the test method and 3D FEM.

Xiang et al. [11] developed a spring-based method for calculating the load distribution by including the bolt hole clearance and the friction effects, but the max error was 12.8% because the contact effect between the bolts and plates was not taken into account. J. Choi and Y. Chun [12] proposed a failure index method to predict the failure loads of mechanically fastened composite joints. The test result differences were well within 10% for all 17 cases.

Dano et al. [13] studied the influence of the two failure criteria to predict the hole elongation and local strain around the holes. The bearing strength is sensitive to the value of the degradation factors selected for the degradation rules. The proposed failure criterions in [12] and [13] did not include the effect of pre-stress due to bolt preload.

Nassar and Yang [14] proposed the mathematical model for the preloaded bolted joint subjected to a transverse loading. The mathematical model accounts the underhead pressure distribution affected by the bolt bending deformation. The correlation among the transverse displacement at the bolt underhead, the transvers shear forces at the underhead bearing.

Nirut and Kitjapat [15] studied the bolt load distributions of a cold-formed steel bolt connection. The experimental study was performed using single-lap shear testing of concentrically loaded bolt connection fabricated from G550 cold-formed steel. The results of the parametric study showed that the thickness ratio controlled the efficiency of the bolt load distribution more than the other parameters such as the bolt diameters.

McCarthy and Gray [16] investigated the effect of varying bolt-torque and bolt-hole clearance on the load distribution in a three-bolt, single-lap joint. Increasing the pre-stress of the two outer bolts tends to balance the load distribution.

Fengrui et al. [17] used the spring-based model to determine the load distribution on bolted single lab joint, the joint stiffness model accounts for the tightening torque and the hole clearance.

Alvaro and Carlos [18] included the three-dimensional stress field and including out-of-plane failure modes in the analytical model to predict composite failure in single-lap bolted. The advantage with respect to other three-dimensional failure criteria is the consideration of non-linear shear stress–strain relationship. They found that the maximum values of fiber failure criterion were located at the lower plies of the laminate. Due to the secondary bending effect, the compressive load exerted by the bolt shank was concentrated on lower plies, thus the through-the-thickness distribution of the fiber failure criterion was non-uniform. Moreover, plies oriented in the longitudinal direction presented higher values of fiber failure criterion.

Olmedo et al. [19] has also included the estimation of secondary bending as a function of geometrical parameters, material properties, and stacking sequence into the bolt stiffness. The secondary bending stiffness, $K_{\emptyset i}$ can be found considering that the joint transmits to the composite plates a transverse load.

$$K_{bolt} = \left[\frac{1}{K_{sh-b}} + \frac{1}{K_{bend-b}} + \frac{1}{K_{be-pl1}} + \frac{1}{K_{\phi 1}} + \frac{1}{K_{be-pl2}} + \frac{1}{K_{\phi 2}}\right]^{-1} \tag{1.1}$$

It has been shown that the estimation of secondary bending as a function of the joint parameters can improve the results obtained using experimental coefficients.

McCarthy et al. [20] modified the mass-spring model to add the effect of clearance. They predicted accurately the load–displacement curve and the load distribution obtained in experimental tests on single-column multi-bolt composite joints. It is shown that even small amounts of clearance can significantly alter the load distribution in the joint.

Gray and McCarthy [21] developed a two-dimensional finite element model of the global bolted joint model (GBJM) for finite element model, where the bolt is represented by a combination of beam elements coupled to rigid contact surfaces. Shell elements are used to model the composite laminates. The GBJM can be used to study the effect of bolt–hole clearance, bolt-torque, friction between laminates, secondary and tertiary bending in the laminates as well as the load distribution in multi-bolt joints. They validated the GBJM using both three-dimensional finite element models and experiments on both single and multi-bolt joints. The GBJM was found to be robust, accurate and highly efficient, with time savings of up to 97% realized over full three-dimensional finite element models.

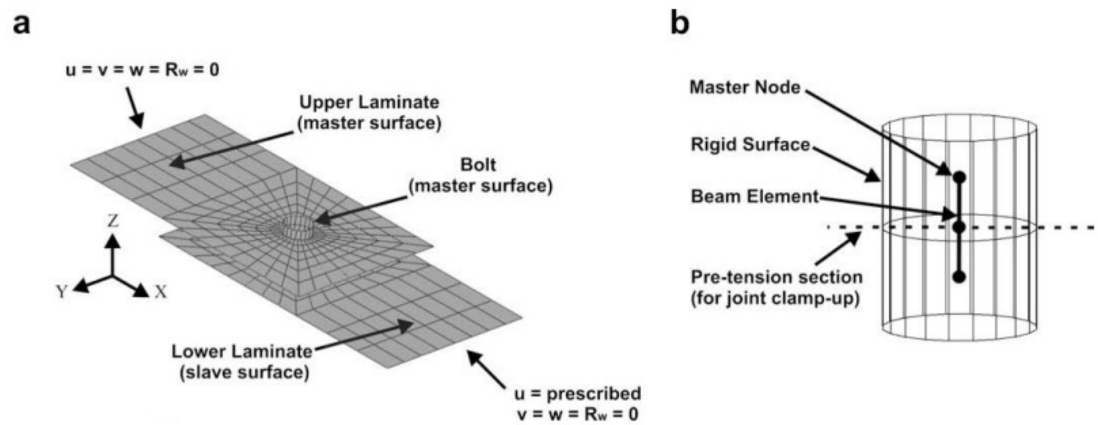

Figure 1.4 Finite element model:(a) mesh of full assembly with boundary conditions and (b) bolt representation [21].

Nelson et al. [22] modified the bolt stiffness to consider the influence of secondary bending on the joint stiffness, an experimental coefficient (b) depending on the bolt configuration was included in the formulation, which was proposed as 0.15 for protruding head joints. The bolt stiffness included the bolt shear stiffness, K_{sh-b}, the bolt bending stiffness, K_{bend-} , the bearing stiffnesses of plates 1 and 2, K_{be-p} .

$$K_{bolt} = \left\{\frac{1}{K_{sh-b}} + \left[\frac{1}{K_{bend-b}} + \frac{1}{K_{be-pl1}} + \frac{1}{K_{be-pl}}\right](1+3b)\right\}^{-1} \quad (1.2)$$

Egan et al. [23] developed the non- linear finite element model of single-bolt, single-lap, countersunk carbon-epoxy joints with variable bolt-hole clearance. The master and slave surfaces in Abaqus code are used to define the contact pairs. They found that where the countersunk hole is oversized, the contact area is reduced, resulting in higher radial stresses, and a reduction in joint stiffness. Reductions in the joint model stiffness correlated reasonably well with the experimental data. Generally, the angled part of the hole was found to be ineffective in transmitting load, and a limited number of plies carried most of the load in the countersunk laminate.

Olmedo et al. [24] used a spring-mass model to reproduce the joint stiffness and a characteristic curve model to predict bearing damage pinned-joint composite laminates by imposing a uniform velocity on the global displacement to calculate the bearing displacement of each ply. The analytical model predictions and the experimental results differences are less than 7%. The main difference is that the analytical model considered the complete failure of the laminate, when experimental tests showed a sudden drop load followed by a new positive load–displacement slope. Bearing damage is a localized mode of failure; hence, after the surface around the hole is damaged, there is an increment of the pin displacement up to the contact with a new composite surface.

McCarthy et al. [25] developed the three-dimensional finite element models to study on the mechanical behavior of bolted composite (graphite/epoxy) joints. The joint type studied was single-bolt, single-lap, which is a standard test configuration in both a civilian and a military standard for composite joints, but the pretension bolt load was not included in the study. The finite element model was constructed in the non-linear finite element code MSC Marc. To improve the model behavior, they increased the element order to second order (20- noded brick elements) and refined both the non-overlap with coarse meshes and overlap regions with fine meshes. The finite element models were also able to capture the effects of secondary bending through-thickness variations in stress and strain.

Following the study of three-dimensional finite element models in single-bolt, single lab joint [25], McCarthy et al. [26] continued their works to study the effects of bolt–

hole clearance on the mechanical behavior of bolted composite (graphite/epoxy) joints. The studied hole clearances were 0 µm (C1), 80 µm (C2), 160 µm (C3) and 240 µm (C4), with a figure tight bolt pretension. The stress contour on the bolt shown that the maximum shear occurred the plane between the two substrates. The larger hole clearance, C4 has a delay since the clearance must be taken up before the bolt makes contact with the hole. But the joint stiffness of tight fit clearance C1 is slightly stiffer than the C4 hole clearance.

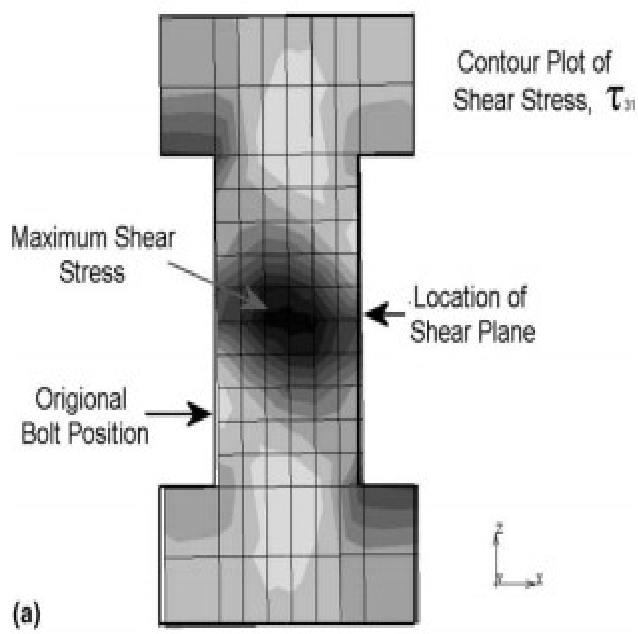

Figure 1.5 Shear Stress distribution C1 clearance joint [26].

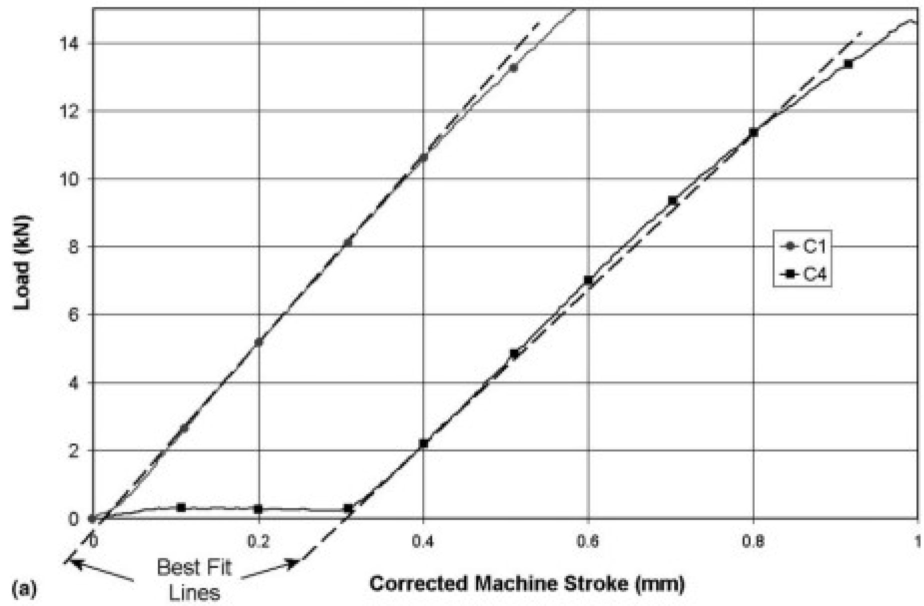

Figure 1.6 Load-displacement curve for C1 and C4 clearance joints (Experimental results) [26].

Fengrui et al. [27] developed the two-dimensional finite element models to for bolt load distribution predictions of composite multi-bolt single-lap joints. In the numerical model, they used the shell element to simulate laminates, the bolts were connected to the shell elements with coupling constraint. The concept of control volume of the bolts and laminates around the holes were used in the model for bolt load distribution analysis. They found that the improved two-dimensional finite element was 0.5% differ from the three-dimensional finite elements and the model predicts secondary bending well, which is an important factor for failure of single-lap joints.

Gray et al. [28] experimentally examined the influence of the bolt diameter to thickness ratio and laminate taper on the stiffness, strength and secondary bending of single-lap, single-bolt, countersunk composite joints. The test setup followed ASTM

D5961/D5961M procedure. With the lower ration of the bolt diameter to the thickness failed at a higher failure load as the bolt-load was distributed over a larger contact area in the thicker joints. In terms of increasing joint thickness, the out-of-plane displacement was less severe in thick joints, which was not immediately obvious since thick joints had higher bending moments due to higher load eccentricity. The bending moment was much lower in the intermediate joint and so, less load was reacted by the nut, thus reducing the likelihood of premature fastener failure.

Junshan et al. [29] studied the effect of the interference fit of single lap bolted composite joints. The shear nonlinearity constitutive relations for composites are defined with the Ramberg Osgood equation. At the low interference-fit level the modeling result shows slight in-plane matrix damage.

José et al. [30] determined the distribution of loads transferred between the different rows of fasteners of single lap, four bolted joints. They used a spring-based model into the analytical model. They validated with analytical model with the three-dimensional model. They found that the higher is the tightening torque, the greater the share of the load sustained by the 2 end lines.

Sharos and McCarthy [31] have developed the novel finite element model to determine the load distribution in a single lap composite joints (1) single bolt joint, (2) a Single-column joint and (3) Triple-column joint, but due to the offset of bearing loads from the shear plane in single-shear joints, the secondary bending moments was also accounted for. The moments about the X-axis were found by multiplying the appropriate component of force by an eccentricity, assumed at the middle of the plates. Under quasi-static loading, tit was very good correlation between the user-element model and experimental data in terms of load-displacement behavior and surface strain measurement.

Awadhani [32] used a simple spring model of a single lap, single bolted compositive joints that was model by Olmedo et al. [24] to study the effect of variation in the joint parameters and bolt tightening torque. It has been observed that the joint stiffness decreases with increase in the length of the plate. The joint stiffness reduces as the diameter of the bolt increases. Also the joint stiffness increase with increase in the width of the plate. The effect of bolt tightening has no significant effect on the joint stiffness.

Johan Ekh and Joakim Schon [33] developed the finite element model to predict the load distribution of a multi-fastener, single-lap, composite-to-aluminum joint. Their model accounts for bolt-hole clearances, bolt clamp loads and member plate frictions. They found that an increased stiffness mismatch between the plates generates a more uneven load distribution, while reducing the length of the overlap region has the opposite effect. Increasing the stiffness of a fastener shifts some of the load from the nearest fasteners to that particular fastener.

Kobyé et al. [34] studied the load sharing of the combination of a bonded joint and bolted joint. The finite element model and experiment was set up with a single-bolt, single-lap composite joint. The bolt was strain gaged to measure the load sharing, and they found the bolt the bolt carrying up to 40% of the overall applied load.

Gordon Kelly [35] also studied the load transfer in a hybrid (bolted/bonded) composite single lap joint by using the finite element model and experimental. He found that the load transferred by the bolt is shown to increase with increasing adhesive thickness. Increasing the thickness of the adhesive in the joint results in a reduction of the shear and peel stresses in the adhesive layer. The shear stress distribution becomes more uniform with no sharp peaks at the ends of the overlap. As the overlap length of the joint is increased, the average shear stress in the center of the joint is reduced with the load transfer mainly occurring in the adhesive at the ends of the overlap.

Barut and Madenci [36] developed the analytical method for the coupled in-plane and bending analysis of composite bonded– bolted single-lap hybrid joints. They used Mindlin and Timoshenko beam theories to determine the laminate and bolt displacements. The bending is mainly due to the force couples created by the lap geometry. They investigated the effects of varying clamp-up forces and the uniaxial and combined loadings. The analysis results show that the clamp-up force induced by the bolt stretching applies compression to the laminates through the bolt heads, causing compressive peeling stresses around the bolt head regions. Furthermore, the presence of the transverse loading significantly changes the distributions of shear and peel stresses in the adhesive. The effect of the increasing debond length on the lap joint is also investigated. It is observed that no bolt load transfer occurs up to a certain debond length. Once the debond length continues to increase beyond this (critical) debond length, the bolt starts to take some of the load. The bolt load transfer rapidly increases and takes the entire load as full debonding occurs in the adhesive.

Kradinov et al. [37] used the variational formulation in conjunction with the complex potential theory to determine the contact stresses and contact region around bolt holes and the bolt load distribution in single-double lap joints of composite laminates with arbitrarily located bolts under general mechanical loading conditions and uniform temperature change. They found that the analytical formulation show excellent correlation with other investigators. The thermal and mechanical loads is significantly different from those arising from the combined loading.

Thomas [38] develop the three-dimensional finite element model of bolted composite joint to determine the non-uniform stress distributions through the thickness of composite laminates in the vicinity of a bolt hole. He validated his numerical model with experiment data by measuring the deformations, strains, and bolt load on test specimens. He also instrumented the gages on the laminates to measure the strain on both sides of the laminates. The comparison between the finite element model and experimental results showed good agreement.

Behrooz et al. [39] used the spring-mass model and nonlinear Tsai-Hahn formula to determine load distribution in single-column multi-bolt composite joints by considering the effect of material nonlinearity of the joint members. They found that by considering material nonlinearity, the displacement increased 3.66% and 3.97% more in comparison to the linear case of three and five bolted joints respectively at the same constant force. In addition, it was shown that increasing the degree of material nonlinearity of the members increased and decreased the amount of the load transferred by the outer and inner bolts of the joint respectively.

Sharos et al. [40] developed an analytical model using a spring mass model to determine the bearing response of multi-bolt composite joints at various loading rates. A single-bolt, single-lap joint was used as the basis for the model, as extensive experimental and numerical studies had been carried out on this configuration. It was shown using the model that for the material and joint configurations considered, strain rate effects associated with the undamaged response of the joint can be neglected for loading velocities up to 10 m/s. However, changes in energy absorption which occur due to increased loading rate cannot. Furthermore, slight variations in the energy absorption characteristics at each fastener hole in a multi-fastener joint can significantly alter the bolt-load distribution in the joint.

Tianliang et al. [41] used combination of experimental and numerical methods to investigate the fastener effect mechanism on the mechanical behavior of double-lap composite joints. The fastener effects on the double-lap joint strength, stiffness and failure mode are de-scribed in detail based on the experiment results. The countersink bolt induces about 32% lower nonlinearity onset strength of the double-lap joint and larger bearing damage around the outer plate hole on bolt head side than protruding head joint. However, the fastener effect on the final strength is very small. Only 4.5% higher rupture strength is found for protruding head joint than that for countersink joint. The initial stiffness of the countersink joint is the same as that of the protruding head joint before damage on set occurs. After the joint stiffness nonlinearity development, the tangential stiffness of countersink joint is slightly higher than that of protruding head joint.

Gordon [42] investigated the strength and fatigue life of hybrid (bonded/bolted) joints with carbon-fiber reinforced plastic adherends. The experimental results shown that the hybrid joints have greater strength, stiffness, and fatigue life in comparison to adhesive bonded joints. However, the benefits were only observed in joints with lower modulus adhesives which allowed for load sharing between the adhesive and the bolt. Hybrid joints with high modulus adhesives showed no significant improvement in strength although increased fatigue life was observed due to the presence of the bolt.

1.3 Motivation

In this research, the beam theory-based model is used to determine the bolt flexibility and uses the spring-based model to calculate the bolt load sharing. Due to the non-uniform load distribution along the bolt shank, the new proposed calibration factors β is applied to an analytical bolt flexibility model, it is obtained from a 3D finite element model. The effect of bolt preloaded F_N and the effect of off-center location of the tensile-shear loading is investigated.

1.4 Objective and Outline

The first objective is to quantify the significance of bolt preload which can affect the bolt load distribution in single lap two bolted joint. The bolt underhead transverse forces due to the bolt pretension loads were included into the analytical model and investigated. The second objective is to investigate the effect of non-central loading for the two-bolt centerline. Due to the substrate geometry tolerances, the tensile loading may not be aligned to the two-bolt centerline. The bolt load sharing among the two bolts may be deviated.

CHAPTER TWO

BEAM THEORY-BASED MODEL OF LOAD TRANSFER IN SINGLE LAP JOINTS

2.1 Force Analysis of the Fastener Under Uniform Load Distribution

The fastener load model over uniform bearing load $w_1 t_1$ and $w_2 t_2$ is simplified as the simple cantilever beam, where one end is fixed as shown in Fig. 2.1, which is a statically indeterminate system.

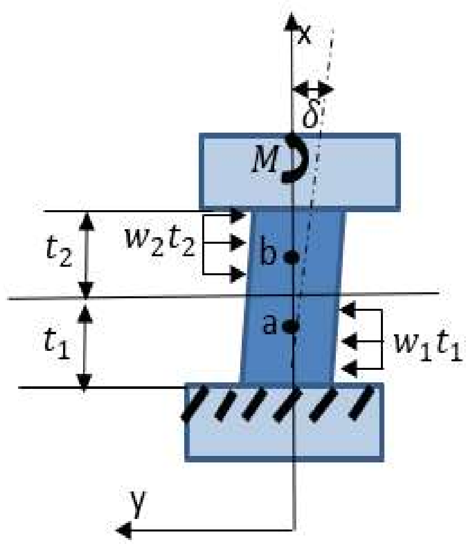

Figure 2.1 Simplified fastener over uniform bearing load.

The angle of rotation of the beam θ_1 under $w_1 t_1$, θ_2 under $w_2 t_2$ and θ_3 under M can be written as following.

$$\theta_1 = \frac{w_1 t_1^3}{6EI} \tag{2.1}$$

$$\theta_2 = \frac{w_2(L^3 - t_1^3)}{6EI} \tag{2.2}$$

$$\theta_3 = \frac{ML}{EI} \tag{2.3}$$

While the rotation angle of the beam on the right equal zero

$$\theta = \theta_1 - \theta_2 + \theta_3 = 0 \tag{2.4}$$

Force equilibrium equation can be written,

$$w_1 t_1 = w_2 t_2 \tag{2.5}$$

Substituting θ_1 , θ_2 , θ_3 from Equation (2.1-2.3) to Equation (2.4)

$$\frac{w_1 t_1^3}{6EI} - \frac{w_2(L^3 - t_1^3)}{6EI} + \frac{ML}{EI} = 0 \tag{2.6}$$

Thus,

$$M = \frac{w_2(2t_1^2 t_2 + 3t_1 t_2^2 + t_2^3)}{6L} \tag{2.7}$$

Fastener Bending Flexibility can be written as following.

$$\delta_{a1} = \frac{w_1 \left(\frac{t_1}{2}\right)^2}{24EI}\left[6t_1^2 - 4t_1\frac{t_1}{2} + \left(\frac{t_1}{2}\right)^2\right] \tag{2.8}$$

$$\delta_{a2} = -\frac{w_2 \left(\frac{t_1}{2}\right)^2}{12EI}\left[3t_2 L + 3t_1 t_2 - 2t_2\frac{t_1}{2}\right] \tag{2.9}$$

$$\delta_{a3} = -\frac{M\left(\frac{t_1}{2}\right)^2}{2EI} \tag{2.10}$$

The total deformation of the point "*a*" is

$$\delta = \delta_{a1} + \delta_{a2} + \delta_{a3} \tag{2.11}$$

Displacements of point "*b*" caused by $F_1 t_1, F_2 t_2$ and *M* can be respectively obtained as

$$\delta_{b1} = \frac{w_1 t_1^3}{24EI}\left[4\left(t_1 + \frac{t_2}{2}\right) - t_1\right] \tag{2.12}$$

$$\begin{aligned}\delta_{b2} = -\frac{w_2}{24EI}\Bigg[&\left(t_1 + \frac{t_2}{2}\right)^4 - 4(t_1 + t_2)\left(t_1 + \frac{t_2}{2}\right)^3 \\ &+ 6(t_1 + t_2)^2\left(t_1 + \frac{t_2}{2}\right)^2 - 4t_1^3(t_1 + \frac{t_2}{2}) + t_1^4\Bigg]\end{aligned} \tag{2.13}$$

$$\delta_{b3} = -\frac{M\left(t_1 + \frac{t_2}{2}\right)^2}{2EI} \tag{2.14}$$

The total deformation of the point "*b*" is

$$\delta = \delta_{b1} + \delta_{b2} + \delta_{b3} \tag{2.15}$$

Thus the bending flexibility of the fastener can be written as

$$C_b = \frac{\delta}{F} = \frac{\delta_b - \delta_a}{F} \tag{2.16}$$

$$C_b = \frac{9t_1^4 + 57t_1^3 t_2 + 96t_1^2 t_2^3 + 57t_1 t_2^3 + 9t_2^4}{384EI(t_1 + t_2)} \tag{2.17}$$

Under the uniform bearing load, the fastener is also subject to the shearing force, so using the Timoshenko beam theory [7], the shear deformation δ between points "*a*" and "*b*" shown in Fig.2.1 can be expressed as

$$\delta = \int \frac{f_s V_u V_L}{G_b A_b} dx \tag{2.18}$$

Where G_b is the shear modulus of the bolt, A_b is the cross-section area of the bolt, f_s is the shape factor of the cylindrical bolt shank, and in this study, $V_u = 1$, $V_L = F_1 t_1 - F_1 x$. The shear displacements of points "*a*" and "*b*" to the shearing plane of the joint, δ_a and δ_{ab} can be respectively expressed as

$$\delta_a = \int_0^{\frac{t_1}{2}} \frac{f_s}{G_b A_b} (F_1 t_1 - F_1 x) dx \tag{2.19}$$

and

$$\delta_b = \int_0^{\frac{t_2}{2}} \frac{f_s}{G_b A_b} (F_2 t_2 - F_2 x) dx \tag{2.20}$$

The total deformation between points "*a*" and "*b*" is

$$\delta = \delta_a + \delta_b \tag{2.21}$$

Since the fastener shanks has round intersection, its shape factor f_s is 10/9 according to Ref. [7]

Substituting $F_1 t_1$, $F_2 t_2$ and f_s into Eq. (2.21), the shear deformation can be obtained as

$$\delta = \frac{5F(t_2 - t_1)}{12 G_b A_b} \tag{2.22}$$

Thus, the shear flexibility of the fastener can be calculated as

$$C_s = \frac{\delta}{F} = \frac{5(t_2 - t_1)}{12 G_b A_b} \tag{2.23}$$

Following Ref. [7], to determine the bearing flexibility of bolts and plates. First, the bearing flexibility of the bolt, the bearing stress (σ_{br}) was defined by the applied load (P) divided by the hole diameter and the plate thickness which is written as Eq. (2.24). The bearing strain (ε_{br}) was defined by the plate bearing displacement divided by the hole diameter which is written using Eq.(2.25).

$$\sigma_{bea} = \frac{P}{Dt} \tag{2.24}$$

$$\varepsilon_{bea} = \frac{\sigma_{bea}}{D} \tag{2.25}$$

$$C_{bbr} = \frac{1}{t_1 E_b} + \frac{1}{t_2 E_b} \tag{2.26}$$

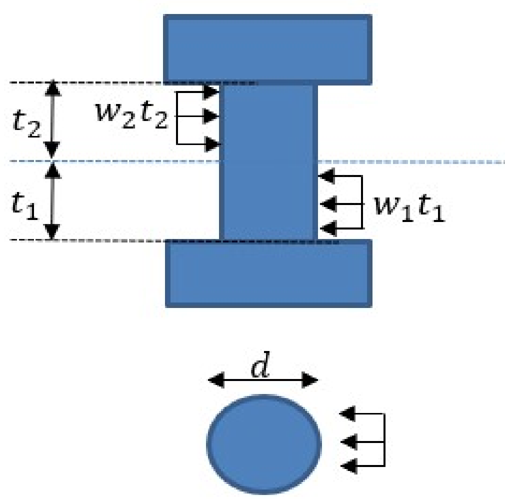

Figure 2.2 Fastener over uniform bearing load

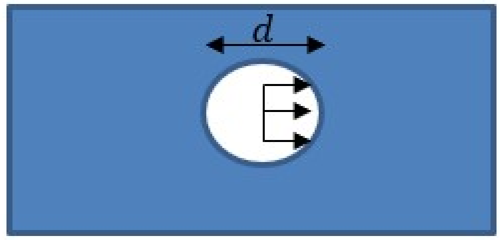

Figure 2.3 Plate over uniform bearing load.

Following the same approach for the two plates, then total plate bearing flexibility is

$$C_{pbr} = \frac{1}{t_1 E_{x1}} + \frac{1}{t_2 E_{x2}} \tag{2.27}$$

Total bolt flexibility can be written as below.

$$C = C_{bb} + C_{bs} + C_{bbr} + C_{pbr} \tag{2.28}$$

$$C = \frac{9t_1^4 + 57t_1^3 t_2 + 96t_1^2 t_2^2 + 57t_1 t_2^3 + 9t_2^4}{384 E_b I (t_1 + t_2)} + \left(\frac{4(t_1 + t_2)}{9 G_b A_b}\right) + \left(\frac{1}{t_1 E_b} + \frac{1}{t_2 E_b}\right) + \left(\frac{1}{t_1 E_{x1}} + \frac{1}{t_2 E_{x2}}\right) \tag{2.29}$$

The bending flexibility of the bolt is caused by the bending moment and bearing loads along the bolt shank. The shearing flexibility is caused by the shearing load along the bolt shanks. The bearing flexibility of the bolt loaded by plate 1 and plate 2 and the bearing flexibility of the plate loaded by the bolt shanks. E_b is Young's modulus of the bolt; E_{x1} and E_{x2} are Young's modulus of the plate 1 and plate 2 in the longitudinal direction; A_b is the cross section area of the bolt; I_b is the moment of inertia of the bolt shank. G_b is the shear modulus of the bolt.

where, $$G_b = \frac{E}{2(1+\vartheta)} \tag{2.30}$$

In the bolt shearing flexibility component, the bolt shear deformation is analyzed and considered the effect of short beam, in which can be written by (10), and it can be ignored when the plate thickness to bolt diameter ratio is greater than 5 as shown in Fig. 2.4.

$$C = \frac{9t_1^4 + 57t_1^3t_2 + 96t_1^2t_2^2 + 57t_1t_2^3 + 9t_2^4}{384EI(t_1+t_2)} + \frac{(t_1+t_2)(1+\vartheta)D^2}{18EI} \tag{2.31}$$

$$C = C_{bb}\left[1 + \frac{64(t_1+t_2)^2(1+\vartheta)D^2}{3(9t_1^4 + 57t_1^3t_2 + 96t_1^2t_2^2 + 57t_1t_2^3 + 9t_2^4)}\right] \tag{2.32}$$

$$C = C_{bb}[1+\psi] \tag{2.33}$$

where,

$$\psi(t_{1,}t_2, D) = \frac{64(t_1+t_2)^2(1+\vartheta)D^2}{27t_1^4 + 171t_1^3t_2 + 288t_1^2t_2^2 + 171t_1t_2^3 + 27t_2^4)} \tag{2.34}$$

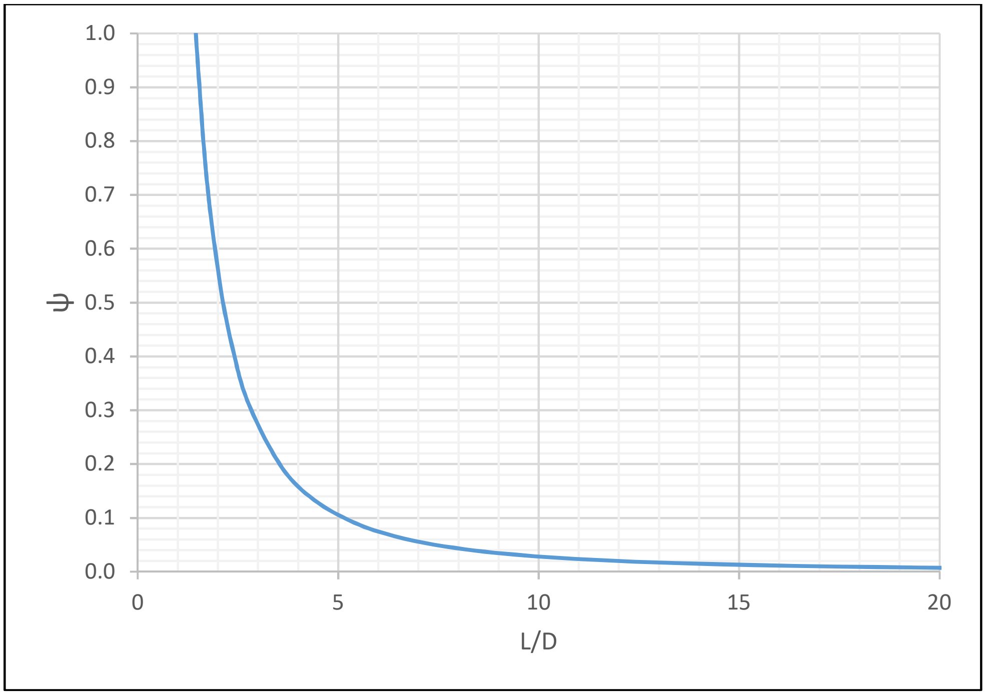

Figure 2.4 Effect of Plate Thickness to Bolt Diameter Ratio.

2.2 Finite Element Analysis Calibration of Analytical Model

Since the contact force is not uniformly distributed along the plate thickness or in another word along a bolt shank, therefore, the 3D finite element model of single lap bolt joint is used to determine the correlation factors $\alpha, \beta, \gamma, \varphi$ separately for each flexibility component. Therefore, Eq. (2.29) can be rewritten as following,

$$C = \frac{9t_1^4 + 57t_1^3t_2 + 96t_1^2t_2^2 + 57t_1t_2^3 + 9t_2^4}{\beta 384 E_b I(t_1 + t_2)} + \alpha\left(\frac{4(t_1 + t_2)}{9G_bA_b}\right) + \gamma\left(\frac{1}{t_1E_b} + \frac{1}{t_2E_b}\right) + \varphi\left(\frac{1}{t_1E_{x1}} + \frac{1}{t_2E_{x2}}\right) \quad (2.35)$$

The bolt and plates parameters are modeled using ABAQUS software shown in Fig.2.5. The thickness of plate 2 varies from 2 mm to 16 mm. One end of the plate is fixed translation, and another end is applied the external tensile load. There are 5 contact pairs defined in the 3D FEA model: (1) bolt head to the top plate, (2) bolt nut to the bottom plate, (3) bolt shank to the hole of the top plate, (4) bolt shank to the hole of the bottom plate and (5) the top plate to the bottom plate shown in Fig.2.6. The 3D hexahedral elements (C3D8R) are used for the simulation.

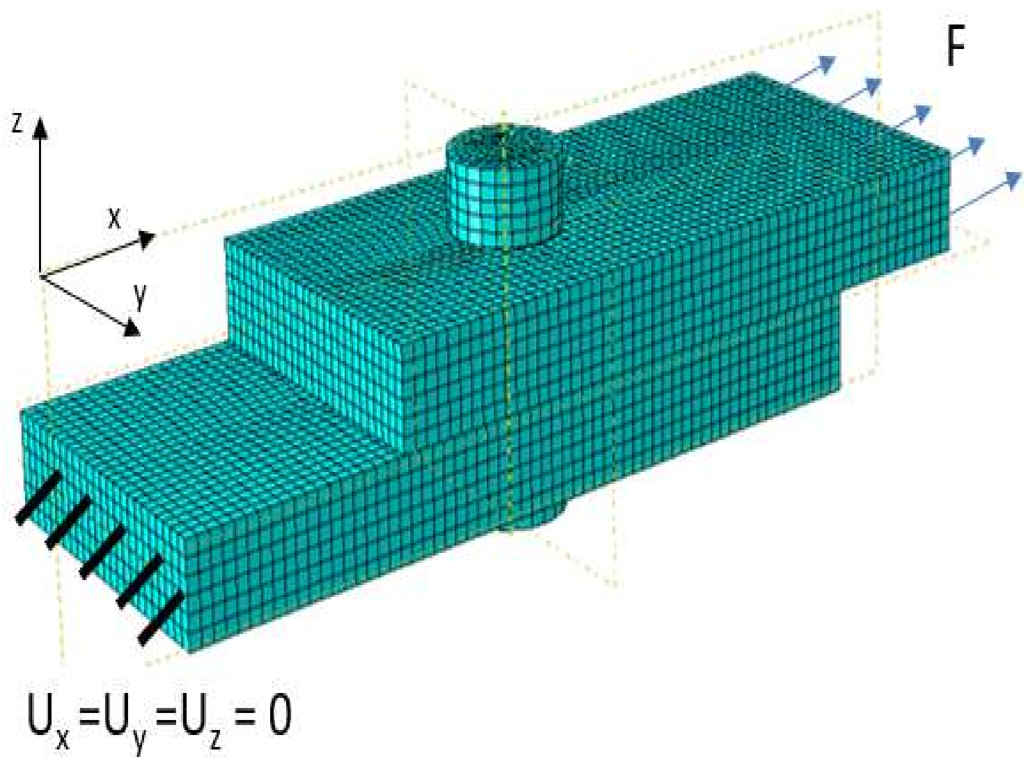

Figure 2.5 3D finite element model of single lap bolt joint calibration model

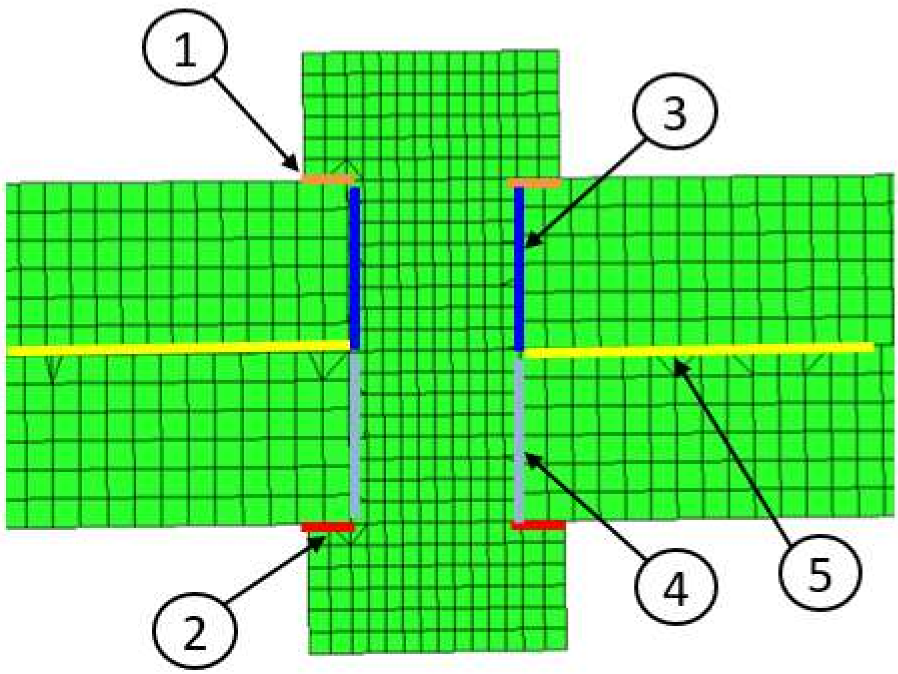

Figure 2.6 3D finite element model- surface contact pairs.

In order to determine the plate flexibility, the elemental nodes inside the plate hole were defined as the node sets as shown in Fig. 2.7. Then the unit load was applied inside the hole surface. The average deformation each node was collected in Fig. 2.8. The plate thicknesses varied from up to 16 mm. The 3D finite element plate flexibility results were corelated to the analytical model to obtain the correlation factor φ. Other correlation factors used the same method to determine the correlation factors α, β, γ separately for each flexibility component.

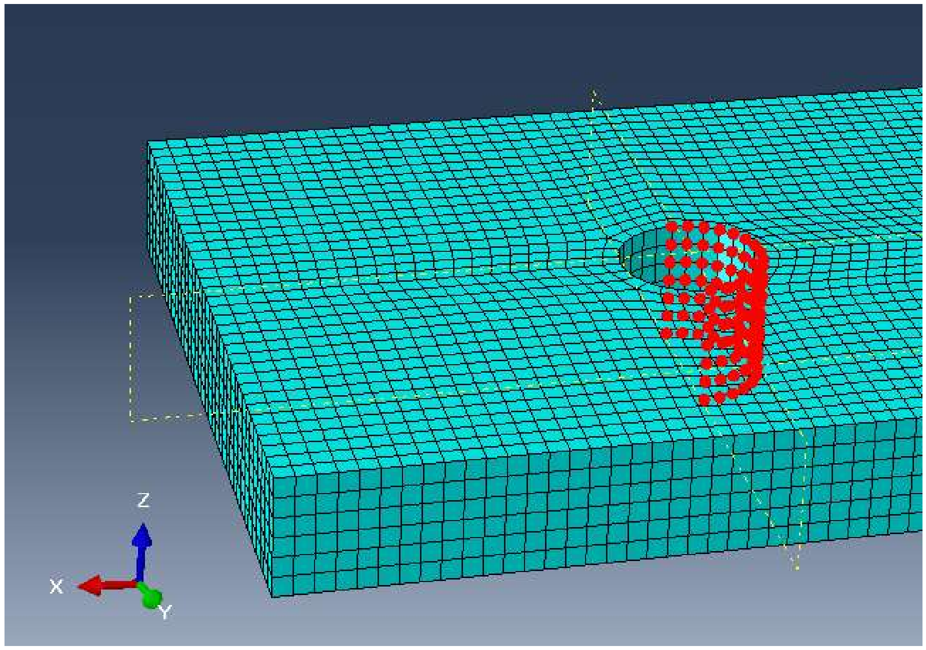

Figure 2.7. 3D finite element model nodal set.

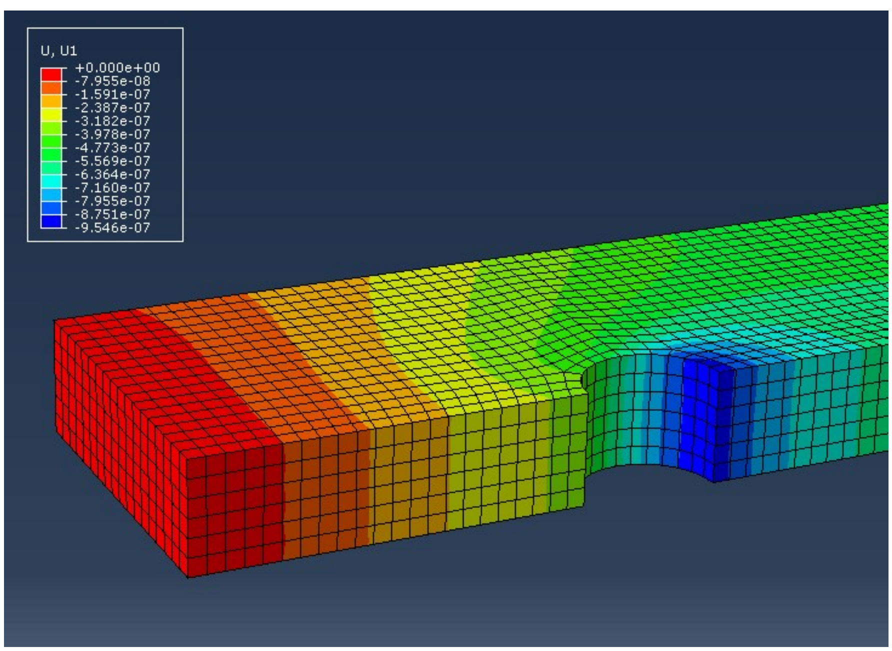

Figure 2.8. 3D finite element model plate deformation.

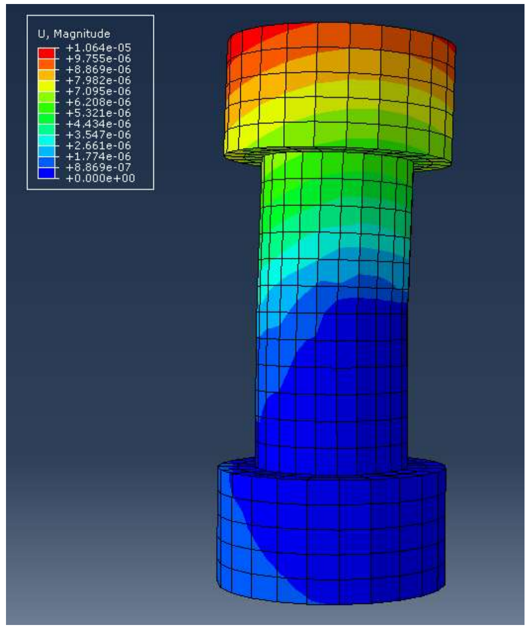

Figure 2.9 3D finite element model bolt deformation.

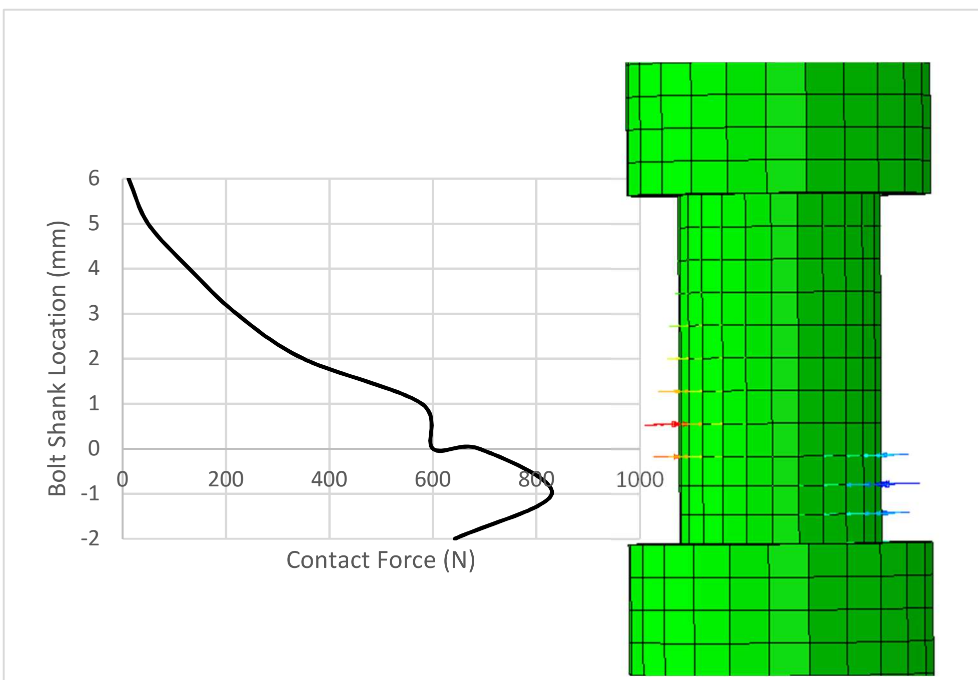

Figure 2.10 Contact Force Distribution (FEA Model, t_2/t_1 = 3)

Based on the 3D FEA result shown in Figure 2.10, with the increase of plate thickness ratio the load distribution is more uneven and concentrates in the area of the interface of the two plates. The proposed new calibration parameter β is dependent on the plate thickness ratio (t_2/t_1) and is given by

$$\beta = \left(\frac{t_2}{t_1}\right)^4 e^{\frac{t_2}{t_1}} \tag{2.36}$$

Other calibration parameters remain unchanged; namely α =0.375, γ=1.15, φ=1.15

2.3 Spring-Mass Model of Single Lap Joints With Two Bolts

Figure 2.11 illustrates a typical single lap joint with two bolts under the tensile shear loading. The left end of the lower substrate is fixed, while the right end of the upper substrate is subjected to the tensile load F in plane parallel to the two plates. The thickness t_1 and t_2 represent the thickness of plate 1 and plate 2 respectively. The distances L_1 and L_2 represent the edge distance of plate 1 to bolt 1 hole center and the plate 2 to bolt 2 hole center respectively. The distance p is the distance between bolt 1 and bolt 2, and W is the plate width.

Lui et al. [7] have simplified the single lap two bolted joint as a spring mass system as shown in Figure 2.12, where one side of a spring mass system is fixed whereas another end is subject to the external tensile shearing loading. The masses are free to move in the longitudinal direction only and the springs have stiffness in the longitudinal direction only. Each nodal mass represents the section of the plates between the two bolts. The spring represents the compliance of each interaction of the plate sections, and the compliance of the bolts. The stiffness of each spring can be determined as following.

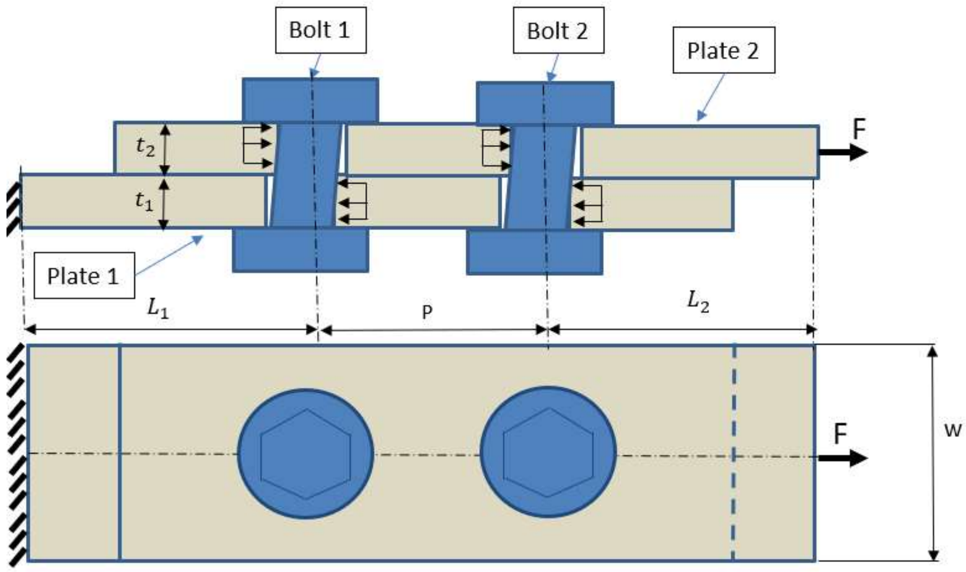

Figure 2.11 Single lap joint with two bolts

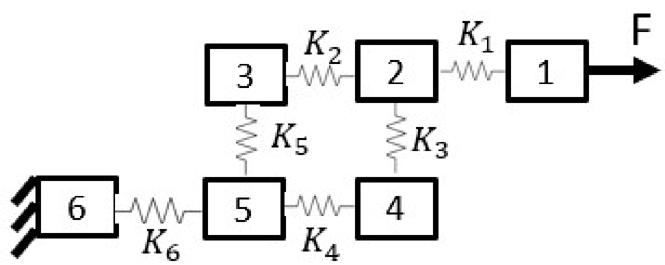

Figure 2.12 Spring Model of single lap joint with two bolts.

K_1 and K_6 are the stiffnesses of the plate sections from the bolts to the ends of the plates which can be calculated by

$$K = \frac{E_x A_{pl}}{l} \tag{2.37}$$

where, E_x is the plate stiffness and A_{pl} is the cross-section area of the plate. K_2 and K_4 are the stiffness of plate sections between the two bolts which can be calculated by

$$K = \frac{E_x A_{pl}}{P} \tag{2.38}$$

K_3 and K_5 are stiffness of bolts in in the single-lap joint. The bolt stiffness was derived by reversing the bolt flexibility using the elastic beam theory with the uniform load distribution per unit length, w_1 andw_2 shown in Fig. 2.1. The bolt flexibility is a summation of the bending flexibility of the bolt, the shearing flexibility of the bolt, the bearing flexibility of the bolt and the plate.

From the mass spring system shown in Fig. 2.12, for quasi-static loading, the system equations can be written a following below, where K_1 and K_6 are stiffnesses of the end plate sections and have a little impact on the bolt load sharing, therefore, when u_5 is threated as zero, the balance equations can be written as a matrix below,

$$\begin{bmatrix} K_1 & -K_1 & 0 & 0 & 0 & 0 \\ -K_1 & K_1+K_2+K_3 & -K_2 & -K_3 & 0 & 0 \\ 0 & -K_2 & K_2+K_5 & 0 & -K_5 & 0 \\ 0 & -K_3 & 0 & K_3+K_4 & -K_4 & 0 \\ 0 & 0 & -K_5 & -K_4 & K_1+K_2+K_3 & -K_6 \\ 0 & 0 & 0 & 0 & -K_6 & K_6 \end{bmatrix} \begin{Bmatrix} u_1 \\ u_2 \\ u_3 \\ u_4 \\ u_5 \\ u_6 \end{Bmatrix} = \begin{Bmatrix} F \\ 0 \\ 0 \\ 0 \\ 0 \\ 0 \end{Bmatrix} \tag{2.39}$$

The nodal deformation was calculated, which gives the P_1 and P_2 bolt load share

$$P_1 = K_5(u_3 - u_5) \tag{2.40}$$

$$P_2 = K_3(u_2 - u_4) \tag{2.41}$$

The total joint displacement u_1 is given by

$$u_1 = \frac{F}{\left(K_2 + K_3 - \frac{K_3^2}{K_3 + K_4} - \frac{K_2^2}{K_2 + K_5}\right)} + \frac{F}{K_1} + \frac{F}{K_6} \tag{2.42}$$

2.4 Finite Element Analysis Verification of Analytical Model

The bolts and plates parameters are modeled using ABAQUS software as shown in Table 2.1 and Fig.2.13. The thickness of plate 2 varies from 2 mm to 16 mm. One end of the plate is fixed translation, and another end is applied the external tensile load. The 3D hexahedral elements (C3D8R) are used for the simulation, the Element size is approximately 0.25 -0.3 mm at the bolt hole and the bolt head and nut areas to obtain more accuracy of contact force. In order to reduce the FEA calculation time, other portion of the plates have 2-3 mm element size as they have less impact to the bolt contact force result. Table 2 shows that the comparison between the analytical and 3D FEA results are in good agreement for all cases within 3% difference.

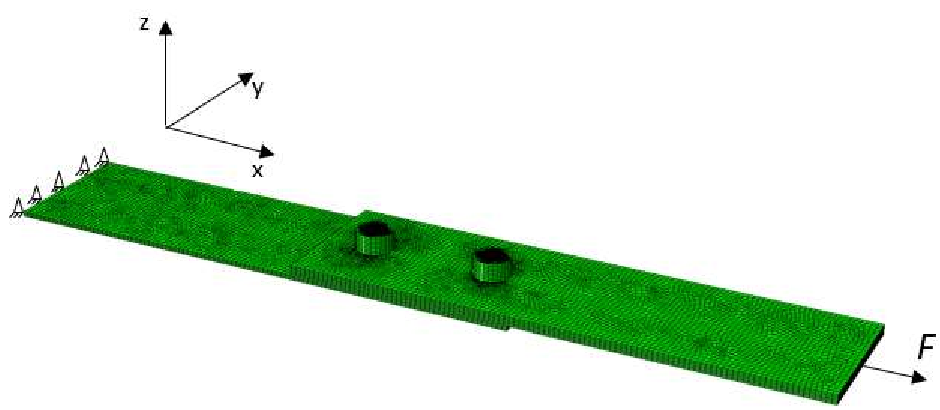

Figure 2.13 3D-FEA Model

Table 2.1 Plate parameters and bolt parameters for Finite Element Model

Parameters of Plate 1				Parameters of Plate 2			
t_1 (mm)	W (mm)	L_1 (mm)	E_1 (MPa)	t_2 (mm)	W (mm)	L_2 (mm)	E_2 (MPa)
2	30	72	196000	2	30	72	196000

Parameters of bolts				
p (mm)	D_1 (mm)	D_2 (mm)	E_3 (MPa)	E_4 (MPa)
25	5	5	196000	196000

Table 2.2 3D-FEA Results.

t_2/t_1	Analytical Results Load Share %		FEA Results Load Share %		Difference %	
	Bolt 1	Bolt 2	Bolt 1	Bolt 2	Bolt 1	Bolt 2
1	50.0	50.0	50.3	49.7	-0.5	0.5
2	52.9	47.1	53.9	46.1	-2.0	2.3
4	55.1	44.9	55.7	44.4	-0.9	1.2
6	56.1	43.9	56.5	43.5	-0.8	1.0
8	56.6	43.4	58.0	42.0	-2.6	3.3

2.5 Results and Discussion

From Figure 2.14 shows that the bolt load distribution difference is greatly increase when the plate thickness ratio increases. This is due to the non-uniform contact load along the bolt shanks and the plate stiffness differences. Figure 2.15 shows the effect of bolt diameter ratio is insignificant to the bolt load distribution, as it can be seen when the bolt 2 diameter increases, the bolt load sharing is only slightly increased. This means that the bolt bearing flexibility and the plate bearing flexibility have very small contribution to the overall bolt flexibility. As shown in Fig. 2.16, the load distribution in bolt 2 will be decreased when the plate width increases; in other words, the plate is stiffer. Furthermore, the effect of bolt spacing distance and the edge distance are not as significant as the width of the plate.

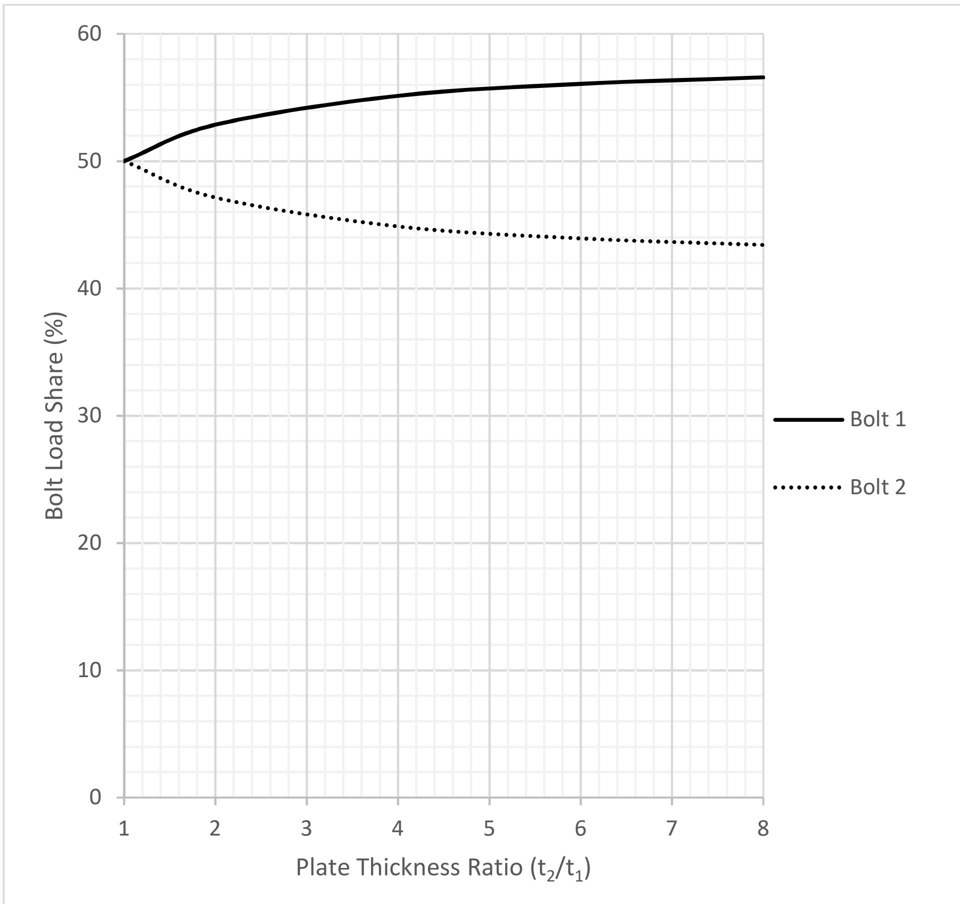

Figure 2.14 Effect of Plate Thickness Ratio (t_2/t_1).

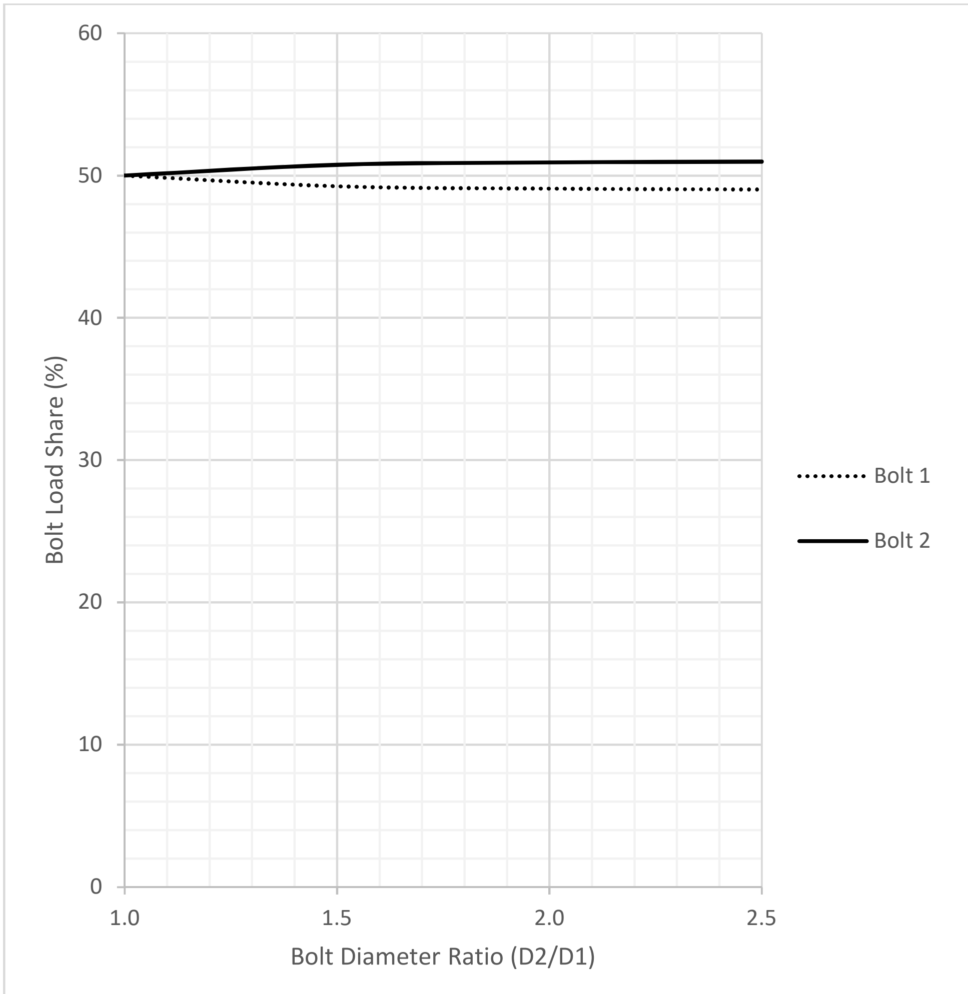

Figure 2.15 Effect of Bolt Diameter Ratio (D_2/D_1).

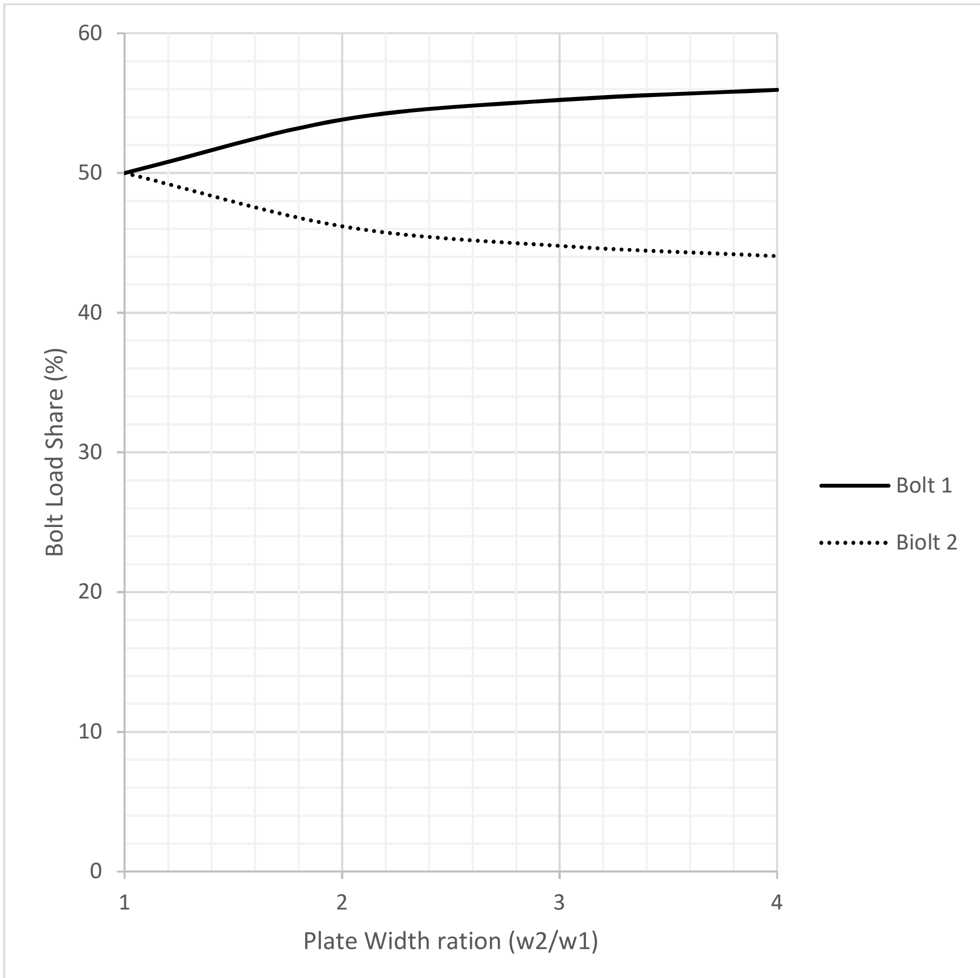

Figure 2.16 Effect of Plate Width Ratio (W_2/W_1).

CHAPTER THREE

EFFECT OF BOLT PRETENSION

3.1 Transverse Forces

When an external shearing tensile load is applied to the single lap joint with preloaded bolts, there will be friction force acting oppositely to the direction of external tensile loading. Bolt underhead contact pressure is non-uniform due to the bending effect of the bolt shank. As the external load increases, the static friction force would eventually be overcome, and joints slipping would start. Subsequently, the bolt shank may come in contact with the bolt hole. At this time, the bolt will carry a sharing external load and the critical friction force.

Nassar and Yang [14], the combined displacement δ due to the bending and the transvers shear force may be express as follows.

$$\delta = \frac{kF_{bs}L^3}{3E_bI_b} \tag{3.1}$$

where the factor k is defined by

$$k = 1 - 3\lambda L\left[4\lambda L + \frac{16E_bI_br_e}{\pi(r_e^4 - r_i^4)}\right] \tag{3.2}$$

Where r_e and r_i are respectively the outer contact radius under bolt head and the internal contact radius under bolt head respectively, L is the effective bolt length, and λ is a constant that is dependent on the bolt underhead bending stiffness. The transvers displacement δ is the sum of the hole clearance and the deflection of the bolt due to the transvers shear force at bolt underhead. The maximum transvers force F_{bs} is the critical friction force that causes the bolt head to slip, it can be defined as below by using the classical Coulomb friction law,

$$F_{bs} = \mu F_N \tag{3.3}$$

where μ is the static friction coefficient, F_N is the normal force or bolt pretension.

Bolt shear loads are equal to the bolt stiffness multiplied by the bolt deflection plus the friction force, which yields

$$P_1 = K_5(u_3 - u_5 - \delta_1) + F_{bs1} \tag{3.4}$$

$$P_2 = K_3(u_2 - u_4 - \delta_2) + F_{bs2} \tag{3.5}$$

3.2 Test Setup

In this section, an experimental procedure and test setup are established for validating the analytical model. The instrumented bolt is designed with two shallow recesses on both sides of the bolt M12 x 1.75 Grade 8.8. Two longitudinal holes are connecting the recesses with the bolt head allowing for connection wires to exit trough the bolt head. The gauges are cemented in the recesses and connected to the lead wires.

Each recess is equipped with one rosette strain gauge and one single axial strain gauge. The rosette strain gauge measures shear, whereas the axial strain gauge measures axial load. All electric wiring and connections are made on top of the head bolt. The signal from the gauges may be connected independently from each other, the necessary bridge being made in the connection to the extension cable at the data-collection computer card.

The rosette gauge type is the Micro Measurements EA-O5-050 RJ120. These are strain rosettes including two strain gauges ±45° to the axial direction positioned equidistant on each side of the faying surface line. The axial strain gauge, Micro Measurements EA-

O5-015 RJ120, is placed parallel to the axial direction and positioned above the rosette gauge shown in Figure 3.1.

The rosette gauges should be connected in a full bridge to eliminate possible bending of the bolt. The axial gauges should be connected in a half bridge for accurate axial measurement. The bolt will be equipped with a total of eight wires. Four of these are external power feed. Two wires are used for measuring shear strain and two for axial strain measurement. The instrumented bolts were calibrated with respect to axial load and shear load. The axial load is obtained by using a special load fixture installed in a tensile test machine shown in Figure 3.3. The load frame is subjected to a tensile load, which introduces a tensile load in the mounted bolt and the corresponding axial strain as shown in Figure 3.4. The shear loading of the bolt will be calibrated by using a single overlap shear joint. The bolt is installed with washers and a finger tight torque. This is to avoid the pre-tension load effect. The plate material in the shear lap joint is made of 1018 steel ASMT A108 with a thickness of 15 mm shown in Figure 3.5 and the plates have the same thickness. The strain gage was instrumented on the bolts close to the shear plane of the two plates. The test is also performed on the tensile test machine. Once the shear loading is applied, the corresponding shear strain is recorded as shown in Figure 3.6. The data shows repeatable and good correlation between the applied shearing loads and the shear strain. Due to the limited instrumented bolts, the calibration process needs to be performed with caution, so the instrumented bolts would not get damaged.

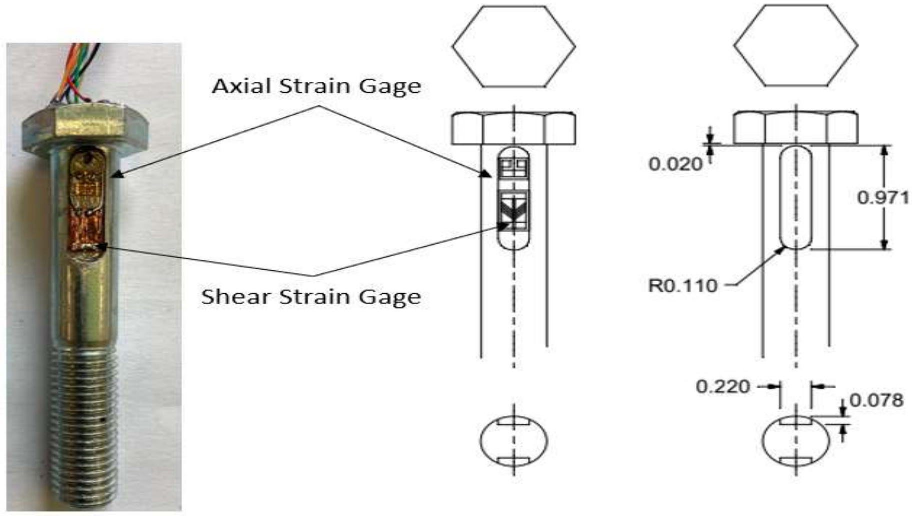

Figure 3.1

MTS 810 (a)

MTS 810 Controller (b)

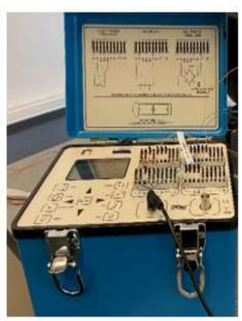

Strain gage indicator (c)

Figure 3.2 Test equipment.

Figure 3.3 Axial strain gage calibration.

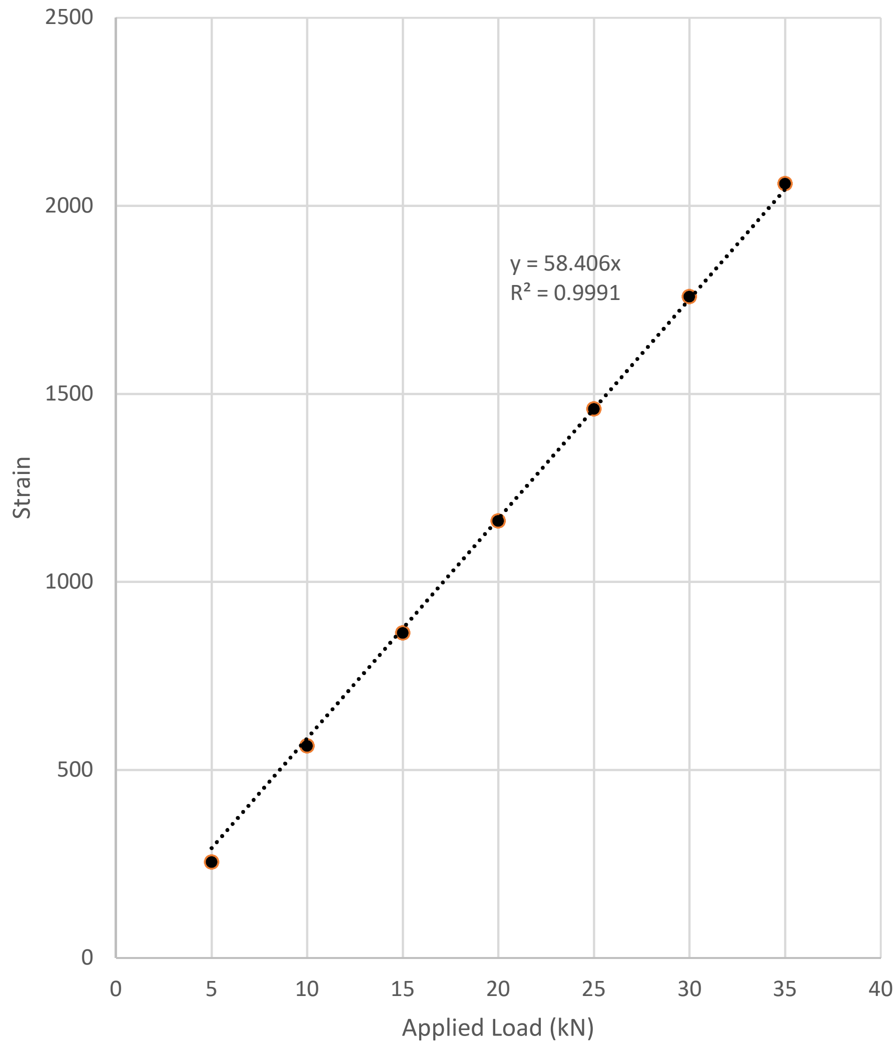

Figure 3.4 Load-strain curve for axial strain gage calibration.

Figure3.5 Shear strain gage calibration.

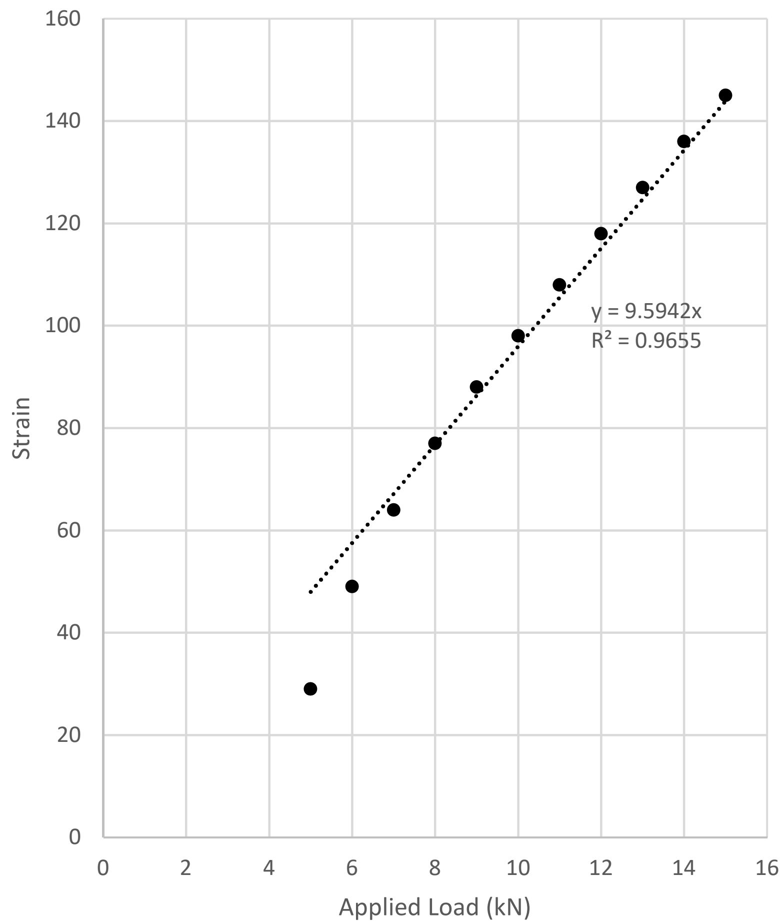

Figure 3. 6 Load-strain curve for shear strain gage calibration.

Table 3.1 Plate geometry parameters

Test No.	W (mm)	L1 = L2 (mm)	P (mm)	t_1 (mm)	t_2 (mm)	D (mm)
1	60	72	60	10	32.57	12
2	60	72	60	10	20	12
3	60	72	60	5	32.57	12

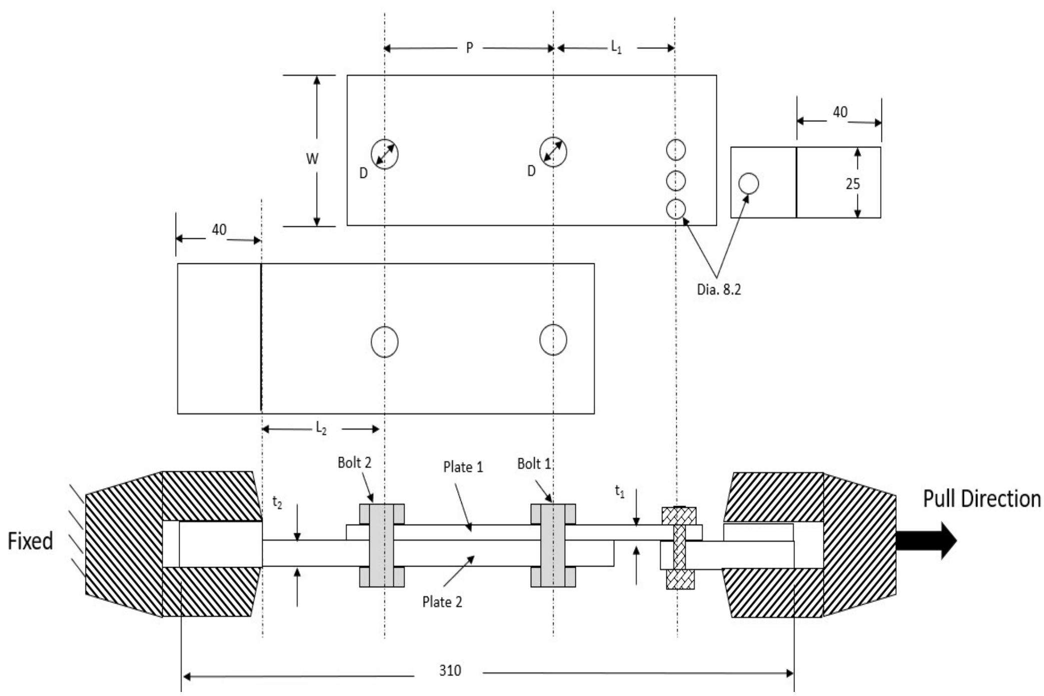

Figure 3.7 Test setup scheme (all dimension in mm).

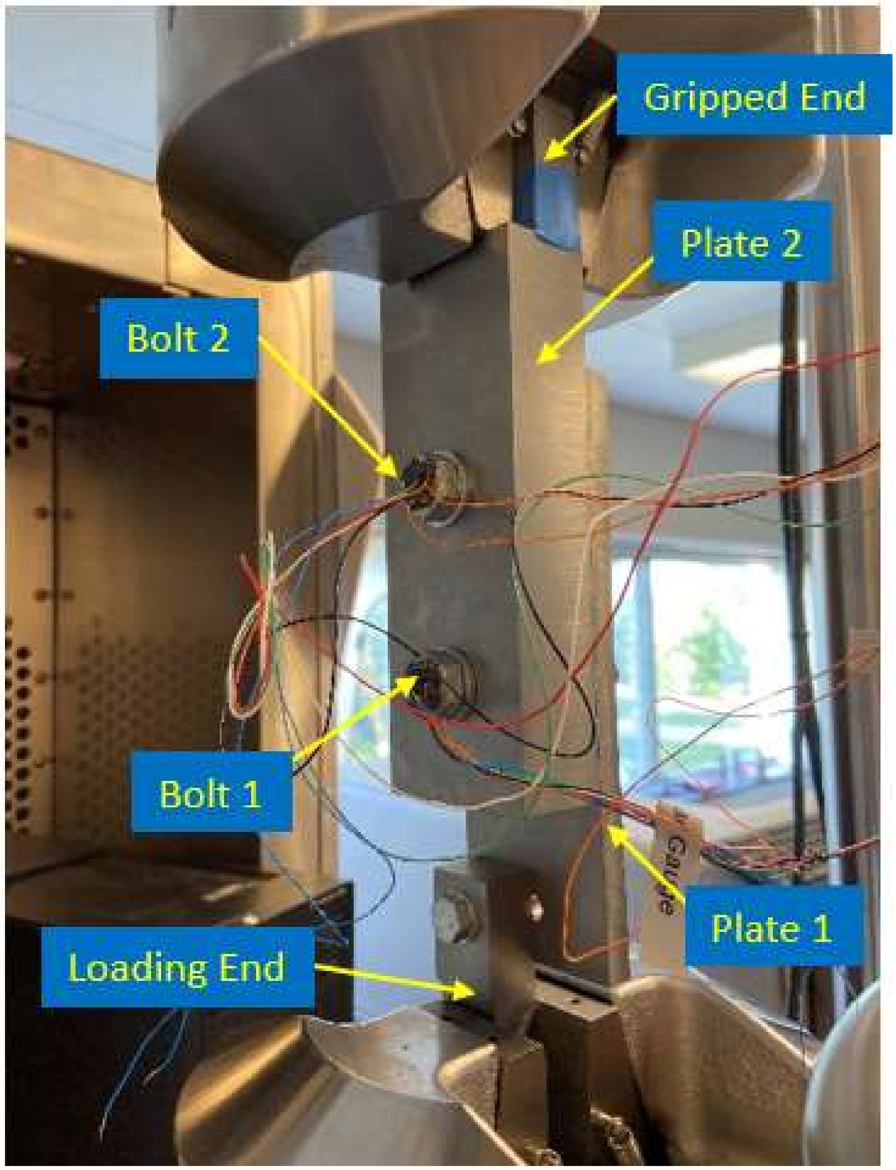

Figure 3.8 Test setup-single lap two bolts

3.3 Results and Discussion

Table 3.2 shows the experimental result compared to the previous researcher, Lui [7]. The test setup is well correlated, and the results are within 3% difference. From Table 3.3 and Figure 3.9 shows that the bolt load distribution difference is greatly increase when the plate thickness ratio increases. This is due to the non-uniform contact load along the bolt shanks and the plate stiffness differences.

Table 3.4 shows that the bolt pretension effects the load sharing between the two bolts but there is not significant. When the external tensile load is applied, the increased of loading is proportional to the joint displacement, however the bolt pretension has no significant effect on the joint stiffness as shown in Fig. 3.11 which agreed with previous literature [32].

Table 3.2 Experimental Verification

Test No	Previous Test Result [7] Load Share %		Current Test Result Load Share %		Difference %	
	Bolt 1	Bolt 2	Bolt 1	Bolt 2	Bolt 1	Bolt 2
1	57.8	42.2	56.5	43.5	-2%	3%

Table 3.3 Test results of plate thickness ratio.

Test No	Plate 1 Thickness (mm)	Plate 2 Thickness (mm)	t_2/t_1	Analytical Results Load Share %		Test Results Load Share %		Difference %	
				Bolt 1	Bolt 2	Bolt 1	Bolt 2	Bolt 1	Bolt 2
1	10	32.57	3.25	54.7	45.3	56.5	43.5	3%	-4%
2	10	20	2.0	53.0	47.0	54.8	45.2	3%	-4%
3	5	32.57	6.5	56.9	43.1	61.7	38.3	8%	-13%

Table 3.4 Test result with various bolt tensions.

Bolt Tension	Analytical Results Load Share %		Test Results Load Share %		Difference %	
	Bolt 1	Bolt 2	Bolt 1	Bolt 2	Bolt 1	Bolt 2
Figure Tight	53.0	47.0	54.8	45.2	3%	-4%
5 kN	52.1	47.9	52.8	47.2	1%	-2%
15 kN	51.6	48.4	53.7	46.3	4%	-5%

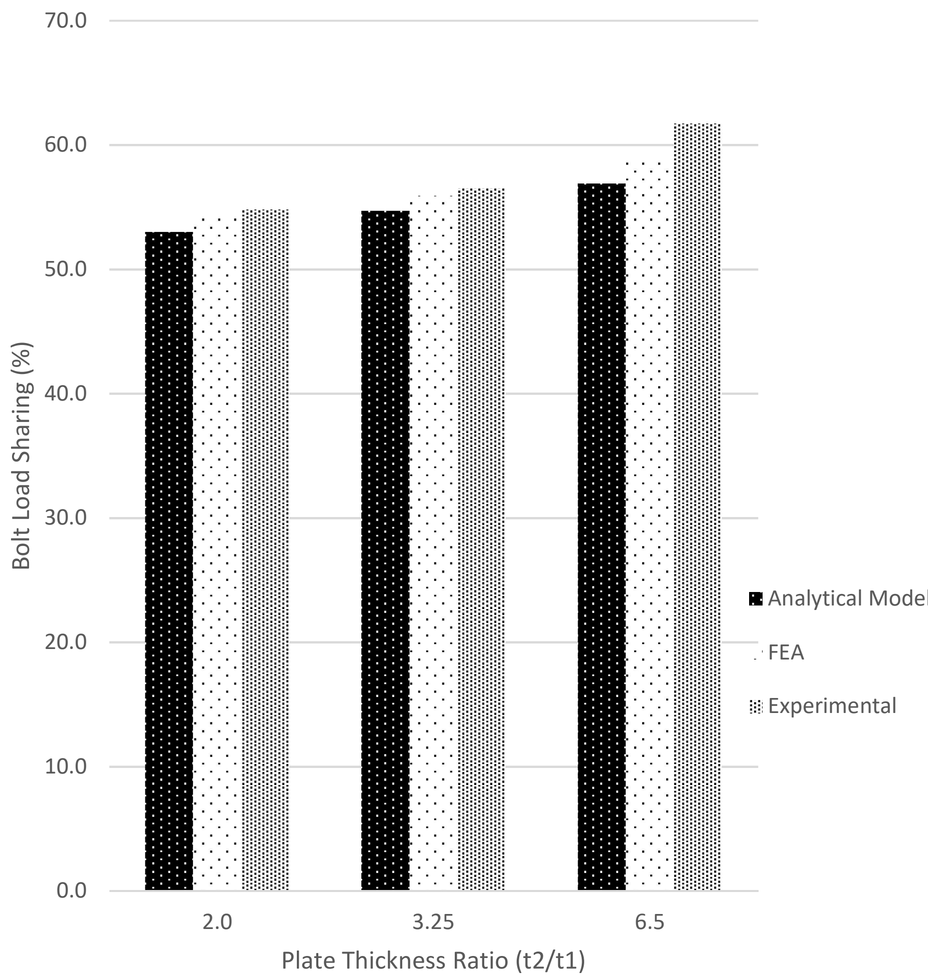

Figure 3.9 Effect of plate thickness Ratio.

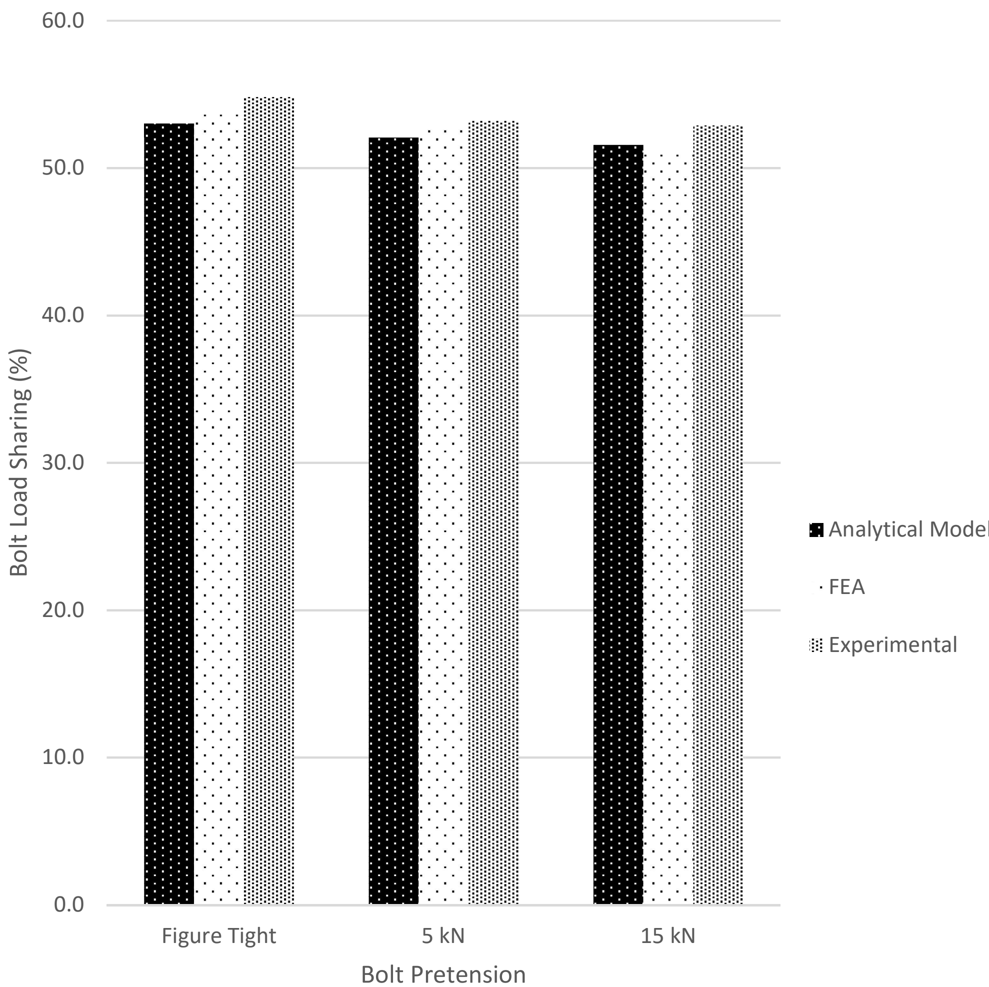

Figure 3.10 Effect of bolt pretension (Test No.2).

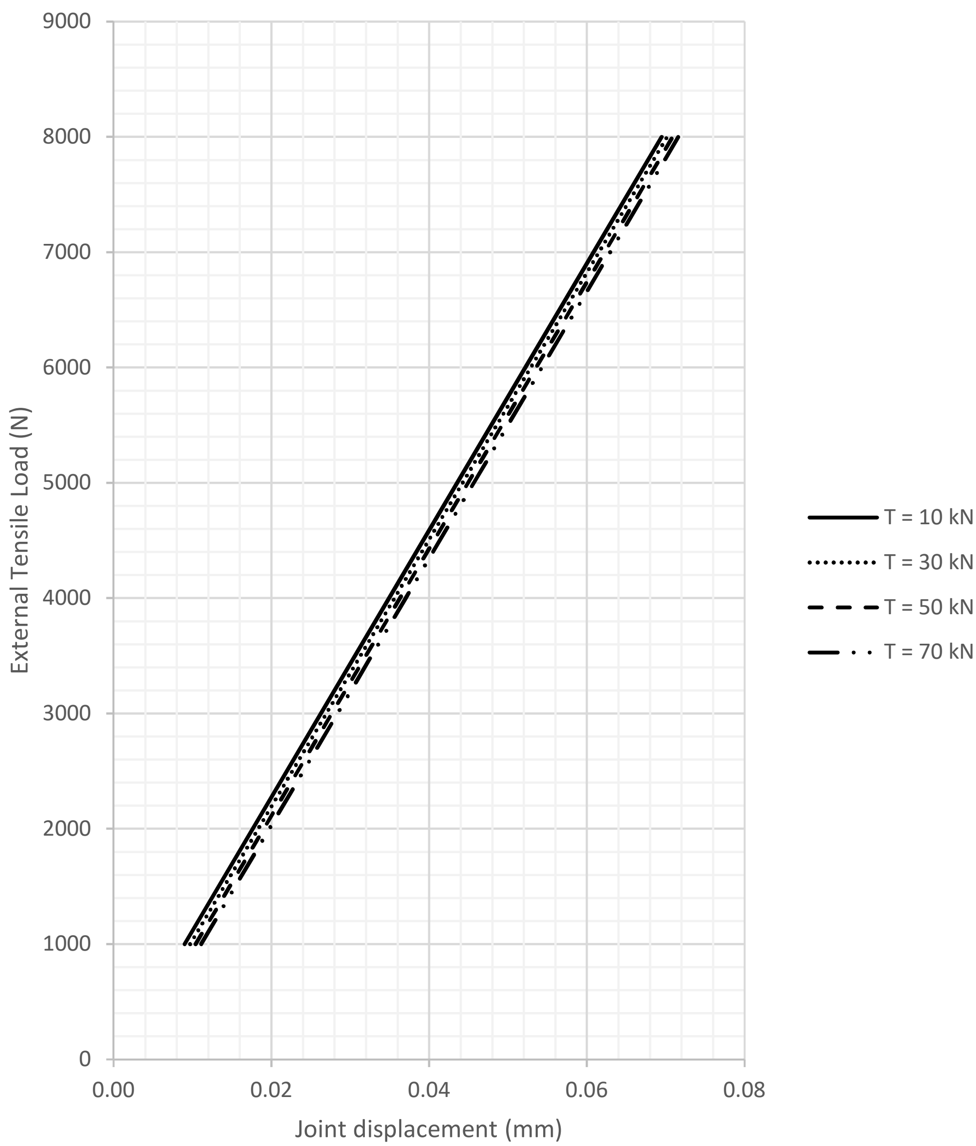

Figure 3.11 Effect of bolt pretension on joint displacement.

CHAPTER FOUR

EFFECT OF NON-CENTRAL TENSILE LOAD

4.1 Non-Central Tensile Load Analysis

When the tensile shear loading is applied offset (e) from the two-bolt center line. The non-central load is converted to an equivalent force system of a load and bending moment, both acting at the center of the two-bolt line. The bolt rotation about the bolt axis is omitted, but the effect of the bending moment will be included the plate longitudinal stiffnesses (K_1,K_2,K_4 and K_6).

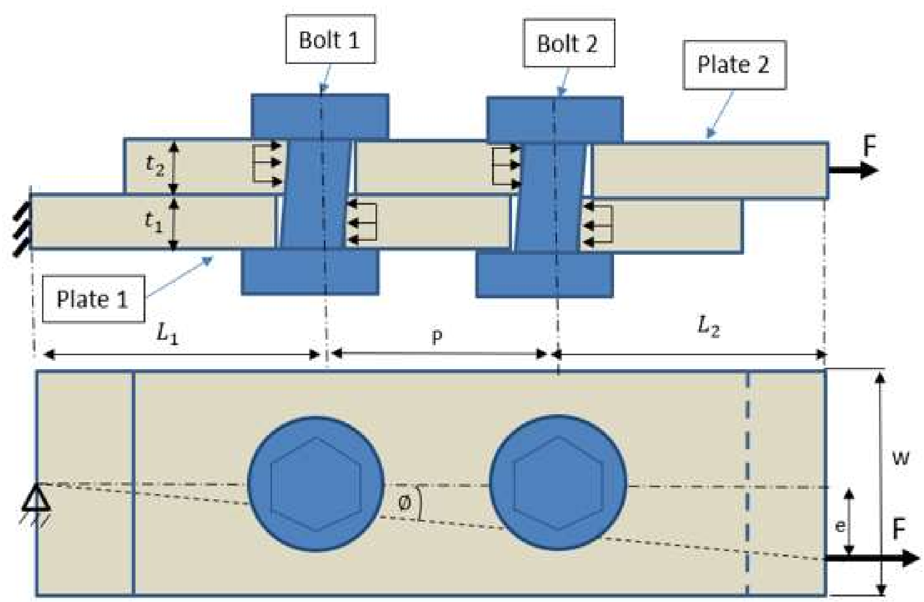

Figure 4.1 Single lap two bolt joint with non-central tensile loading.

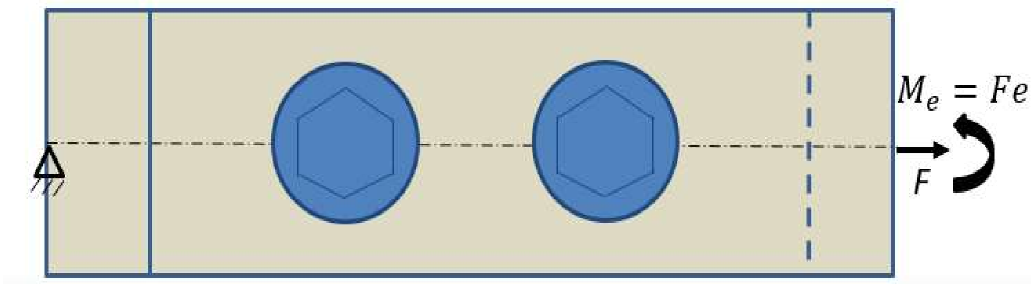

Figure 4.2 Equivalent force system of a non-central tensile loading.

From the elastic beam theory, the normal stresses due to the axial force and bending moment can be obtained as

$$\sigma_a = \frac{F}{A_{pl}} \tag{4.1}$$

$$\sigma_b = \frac{(Fe)\frac{w}{2}}{I_p} \tag{4.2}$$

$$\sigma_b = \frac{F(L_1 + L_2 + P)\tan\theta\left(\frac{w}{2}\right)}{I_p} \tag{4.3}$$

Assuming the average longitudinal deflection of the plate is caused by the combined normal stresses above; where the bending stress is averaged across the plate section, then the individual stiffness of plates can be calculated as

$$\sigma_{avg} = F\left(\frac{1}{A_{pl}} + \frac{w(L_1 + L_2 + P)\tan\theta}{4I_p}\right) \tag{4.4}$$

$$K_p = \frac{E_x}{L\left(\frac{1}{A_{pl}} + \frac{w(L_1 + L_2 + P)\tan\theta}{4I_p}\right)} \tag{4.5}$$

Recalculate Eq. (2.37) thru Eq. (2.39) and determine the bolt load distribution each bolt and the joint displacement.

4.2 Test Setup

Figure 3.8 in Chapter 3 shows a test setup on the tensile test machine. The two different plate thicknesses bolted with two M12 bolts. The plate thickness varies from 5 mm, 10 mm, 20 mm and 32.57 mm. The plate 1 has three additional 8.2 mm diameter holes at another end which is used to mount to the fixture adapter with M8 bolt. Each hole has 12 mm spacing. This allows the loading gripper be pulled offset from the two bolt center line shown in Figure 4.3. varies from 0 degree (no offset), 3.4 degree and 6.7 degree.

At the gripper ends, the test fixture thicknesses were designed to have the same thickness and the tensile shearing loads to be applied at the shearing plane. This is to avoid the tensile machine test faulty due to the out of planed loading. The tests were performed with the finger tight, 10 kN and 15 kN pretension. The external tensile shearing loading was applied incrementally 5 kN, 10 kN, and 15kN. Once the load was applied the strain value from each instrumented bolts from the strain gage reader were recorded. The strain values were correlated to the shearing load by using the shear strain calibration curve in Fig. 3.6. The load sharing for a single lap, two bolted joints are determined for each test configuration, and presented as following figures.

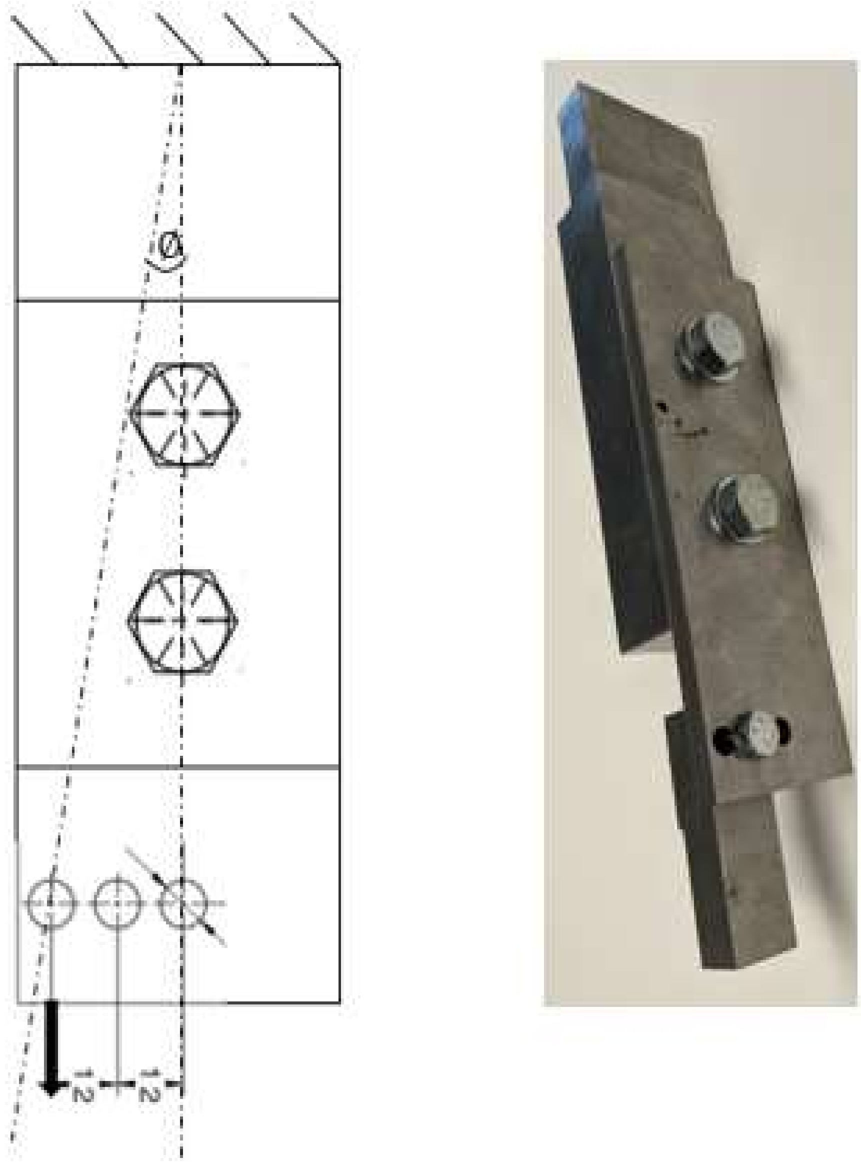

Figure 4.3 Scheme of test set up for non-central tensile loading.

4.3 Results and Discussion

With the plate thickness difference, the non-central tensile loading effects the bolt load sharing as shown in Table 4.1 and Figure 4.4. The higher non-central tensile loading distance makes the greater in the bolt load distribution difference. In Fig. 4.5, it indicates that the additional bending moment due to a non-central tensile loading influences the joint system displacement.

Table 4.1 Test result with various plate offset.

Offset (Degree)	Analytical Results Load Share %		Test Results Load Share %		Difference %	
	Bolt 1	Bolt 2	Bolt 1	Bolt 2	Bolt 1	Bolt 2
0	54.7	45.3	56.5	43.5	3%	-4%
3.4	61.9	38.1	60.8	39.2	-2%	3%
6.7	64.8	35.2	66.1	33.9	2%	-4%

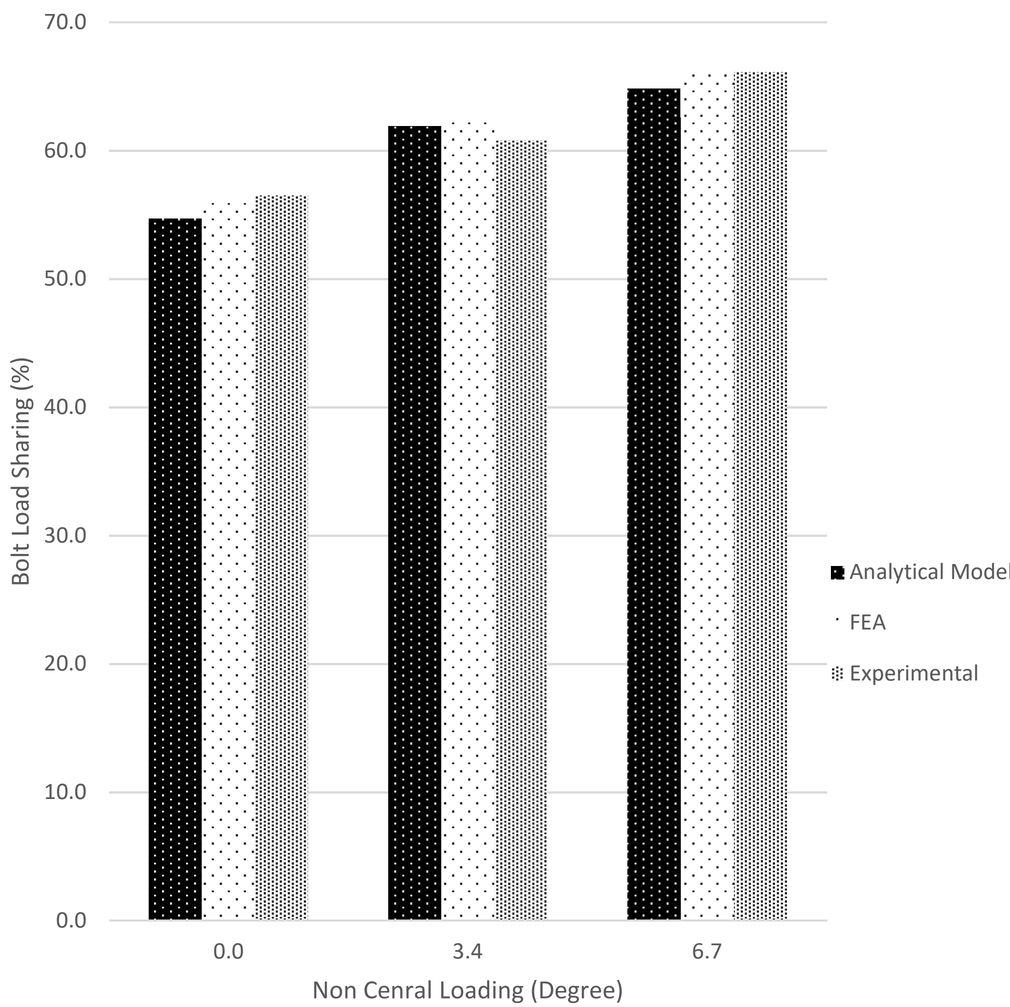

Figure 4.4 Effect of non-central loading

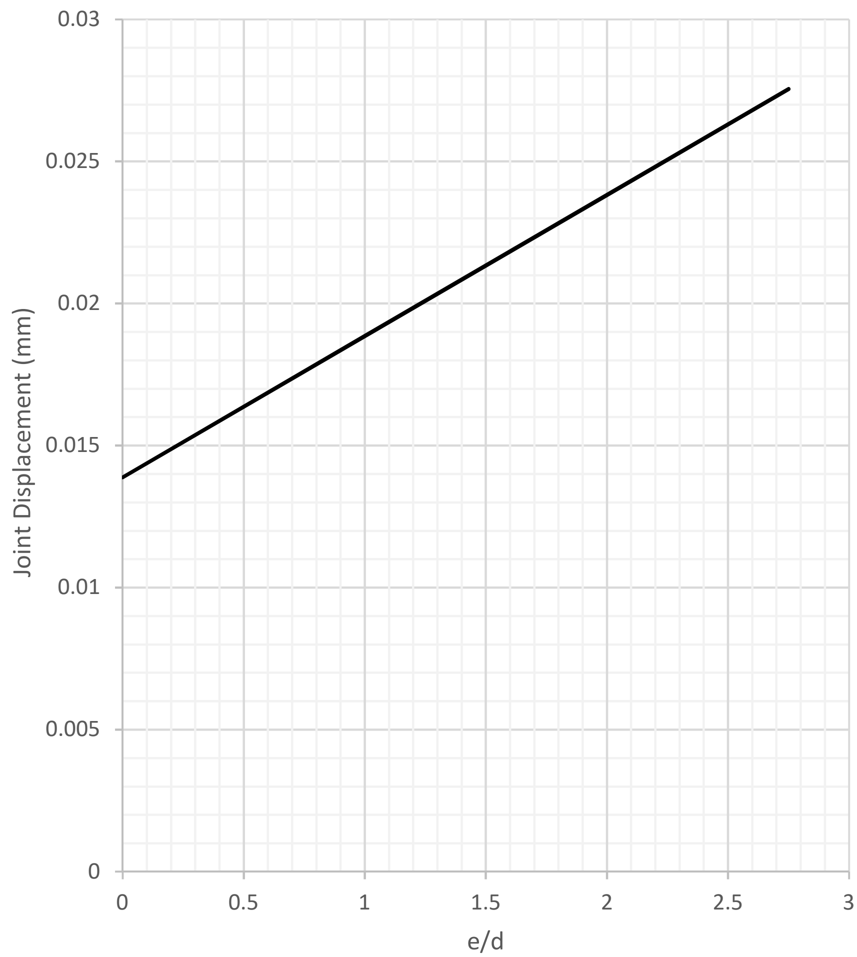

Figure 4.5 Effect of non-central distance (e/d) on Joint displacement.

CHAPTER FIVE

CONCLUSION

5.1 Conclusion

An analytical model for the load distribution in a single lap two bolt joint was developed using the spring mass-based model. The bolt stiffness was derived by using a simplified beam model. Due to the non-uniform load distribution on the bolt, the analytical model was calibrated by using the 3D finite element analysis. The proposed calibration factors α, β, γ and φ were obtained.

The analytical model results, the 3D finite element analysis and the experiment were performed and discussed. The increase in plate thickness ratio and the plate width has more impact to the bolt load sharing than the bolt diameter, the bolt spacing distance and the plate edge distance.

When the bolt pretensions are applied to the bolts, the effect of friction forces and bolt underhead deflections are influent the load sharing, but not significant.

In the situation of the tensile shear loading is applied offset to the bolt centerline, the additional bending has significant effect to the load distribution when the two plates have different thicknesses. The non-central loading distance will also increase the overall joint displacement.

REFERENCES

[1] Khashaba, U.A., Sallam, H.E.M. , Al-Shorbagy, A.E., Seif, M.A., 2006, "Effect of washer size and tightening torque on the performance of bolted joints in composite structures," Elsevier Science Ltd, Composite Structures 73, pp. 310–317.

[2] Pakdil, M., 2009, "Failure analysis of composite single bolted-joint subjected to bolt pretension," Indian Journal of Engineering & Materials Sciences, Vol.16, pp. 79-85.

[3] Kweon, J.H., Jung, J.W., Kim, T.H., Choi, J.H., Kim, D.H., 2006 "Failure of carbon composite-to-aluminum joints with combined mechanical fastening and adhesive bonding," Elsevier Science Ltd, Composite Structures 75, pp. 192-198.

[4] McCarthy, M.A., Lawlor, V.P., Stanley, W.F., McCarthy, C.T., 2002, "Bolt-hole clearance effects and strength criteria in single-bolt, single-lap, composite bolted joints," Elsevier Science Ltd, Composites Science and Technology 62, pp. 1415–1431.

[5] McCarthy, M.A., Lawlor, V.P., Stanley, W.F., 2009, "An experimental study of bolt–hole clearance effects in single-lap, multibolt composite joints", Journal of Composite Materials, Vol. 39, No. 9, pp. 799-825

[6] Stocchi, C., Robinson, P., Pinho, S.T., 2011, "A detailed finite element investigation of composite bolted joints with countersunk fasteners," 18th International Conference on Composite Materials.

[7] Liu, L., Mao, Y., Wei, R., 2011, "An analytical tool to predict load distribution of multi-bolt single-lap thick laminate joints," 18th International Conference on Composite Materials.

[8] Liu, F., Lu, X., Zhao, L., Zhang, J., Hu, N., Xu, J., 2018, "An interpretation of the load distributions in highly torqued single-lap composite bolted joints with bolt-hole clearances," Elsevier Science Ltd, Composite Part B 138, pp. 194-205.

[9] Yeh, H.-Y., Lee, J.J., and Yang, D.Y.T., 2004, "Study of multirow highly loaded bolt joints in composite wing structure," Journal of Aircraft Vol.41, No.2, pp.380-385.

[10] Liu, L., Chen, K., Zhang, J., 2014, "Numerical method on load sharing problem of think laminate joints," J. Shanghai Jiaotong Univ. (Sci), Vol. 19(1), pp. 95-101.

[11] Xiang, J., Zhao, S., Li, D., Wu, Y., 2017, "An improved spring method for calculating the load distribution in multi-bolt composite joints," Elsevier Science Ltd, Composite Part B 117, pp. 1-8.

[12] Choi, J.H., Chun, Y.J., 2003, “Failure load prediction of mechanically fastened composite joints,” Journal of Composite Material, Vol. 37, pp. 2163-2177.

[13] Dano, M. L., Kamal, E., Gendron, G., 2007, “Analysis of bolted joints in composite laminates: Strain and bearing stiffness predictions,” Elsevier Science Ltd, Composite Structures 79, pp. 562–570.

[14] Nassar, S. and Yang, X., 2009, “A mathematical model for vibration-induced loosening of preloaded threaded fasteners,” Journal of Vibration and Acoustics, Vol.131, pp. 021009-1 – 021009-13.

[15] Nirut, K. and Kitjapat, P., 2017, “An analytical method for determining the load distribution of single-column multibolt connection,” Hindawi- Advances in Civil Engineering, Vol. 2017, Article ID 1912724.

[16] McCarty, C.T. and Gray, P.J., 2010, “An analytical model for the prediction of load distribution in highly torqued multi-bolt composite joints,” Journal of Composite Structures, Vol. 93, Issue 2, pp.287-298.

[17] Fengrui, L., Jianyu, Z., Libin, Z., An, X., Longwei, Z., 2015, “An analytical joint stiffness model for load transfer analysis in highly torqued multi-bolt composite joints with clearances,” Journal of Composite Structures, Vol. 131, pp. 625-636.

[18] Álvaro, O. and Carlos, S., 2012 “On the prediction of bolted single-lap composite joints,” Journal of Composite Structures, Vol. 94, pp. 2110-2117.

[19] Olmedo, A., Santiuste, C., Barbero, E., 2014, “An analytical model for the secondary bending prediction in single-lap composite bolted-joints,” Journal of Composite Structures, Vol. 111, pp. 354-361.

[20] McCarthy, M.A., McCarthy, C.T., Padhi, G.S., 2006, “A simple method for determining the effects of bolt–hole clearance on load distribution in single-column multi-bolt composite joints,” Journal of Composite Structures, Vol. 73, pp. 78-87.

[21] Gray, P.J. and McCarty, C.T., 2010, “A global bolted joint model for finite element analysis of load distributions,” Journal of Composites, Part B 41, pp.317-325.

[22] Nelson, W.D., Bunin, B.L., Hart-Smith, L.J., 1983,” Critical joints in large composite aircraft structure,” NASA CR-3710.

[23] Egan, B., McCarthy, C.T., McCarthy, M.A., Frizzell, R.M., 2012, “Stress analysis of single-bolt, single-lap, countersunk composite joints with variable bolt-hole clearance,” Journal of Composite Structures, Vol. 94, pp.1038-1051.

[24] Olmedo, A., Santiuste, C., Barbero, E., 2014, "An analytical model for predicting the stiffness and strength of pinned-joint composite laminates," Journal of Composites Science and Technology, Vol. 90, pp.67-73.

[25] McCarthy, M.A., McCarthy, C.T., Lawlor, V.P., Stanley, W.F., 2005, "Three-dimensional finite element analysis of single-bolt, single-lap composite bolted joints: part I—model development and validation," Journal of Composite Structures, Vol. 71, pp. 140-158.

[26] McCarthy, C.T., McCarthy, M.A., 2005, "Three-dimensional finite element analysis of single-bolt, single-lap composite bolted joints: Part II—effects of bolt-hole clearance," Journal of Composite Structures, Vol. 71, pp. 159-175.

[27] Liu, F., Yao, W., Zhao, L. Wu, H., Zhang, X., Zhang, J., 2020, "An improved 2D finite element model for bolt load distribution analysis of composite multi-bolt single-lap joints," Journal of Composites, Vol. 253, 112770.

[28] Gray, P.J., O'Higgins, R.M., McCarthy, C.T., 2014, "Effect of thickness and laminate taper on the stiffness, strength and secondary bending of single-lap, single-bolt countersunk composite joints," Journal of Composite Structures, Vol. 104, pp. 315-324.

[29] Hua, J., Zhanga, K., Xub, Y., Chenga, H., Xua, G., Lia, H., 2019, "Modeling on bearing behavior and damage evolution of single-lap bolted composite interference-fit joints," Journal of Composites, Volume 212, pp.452-464.

[30] Andriamampianina, J., Alkatan, F., Stéphan, P., Guillot, J., 2012, "Determining load distribution between the different rows of fasteners of a hybrid load transfer bolted joint assembly," Journal of Aerospace Science and Technology, vol. 23, pp.312-320.

[31] Sharos, P.A., McCarthy, C.T., 2020, "Novel finite element for near real-time design decisions in multi-fastener composite bolted joints under various loading rates," Journal of Composite Structures, Vol. 220, 112005.

[32] Awadhani, L.V., 2017, "Parametric Study of Single Bolted Composite Bolted Joint Subjected to Static Tensile Loading," Conf. Series: Material Science and Engineering, ICMAEM-2017-012215.

[33] Ekh, J., Schon, J., 2008, "Finite element modeling and optimization of load transfer in multi-fastener joints using structural elements," Composite Structures, Vol. 82, pp.245-256.

[34] Bodjona, K., Raju, K., Lim, G.H., Lessard, L., 2015, "Load sharing in single-lap bonded/bolted composite joints. Part I: Model development and validation," Composite Structures, Vol.129, pp.268-275.

[35] Kelly, G., 2005, "Load transfer in hybrid (bonded/bolted) composite single-lap joints," Composite Structures, Vol.69, pp.35-43.

[36] Barut, A., Madenci, E., 2009, "Analysis of bolted–bonded composite single-lap joints under combined in-plane and transverse loading," Composite Structures, Vol. 88, pp.579-594.

[37] Kradinov, V., Barut, A., Madenci, E., Amber, D.R., 2001, "Bolted double-lap composite joints under mechanical and thermal loading," International Journal of Solids and Structures, Vol. 38, pp.7801-7837.

[38] Ireman, T. 1998, "Three-dimensional stress analysis of bolted single-lap composite joints," Composite Structures, Vol. 43, pp.195-216.

[39] Taheri, F., Shamaei, A.R., Hefzabad, R.N., 2015, "Effects of material nonlinearity on load distribution in multi-bolt composite joints," Composite Structures, Vol. 125, pp.195-201.

[40] Sharos, P.A., Egan, B., McCarthy, C.T., 2014, "An analytical model for strength prediction in multi-bolt composite joints at various loading rates," Composite Structures, Vol. 116, pp.300-310.

[41] Qin, T., Zhao, L., Zhang, J., 2013, "Fastener effects on mechanical behaviors of double-lap composite joints," Composite Structures, Vol. 100, pp.413-423.

[42] Kelly, G. 2006, "Quasi-static strength and fatigue life of hybrid (bonded/bolted) composite single-lap joints," Composite Structures, Vol. 72, pp.119-129.